

PDF hosted at the Radboud Repository of the Radboud University Nijmegen

The following full text is a publisher's version.

For additional information about this publication click this link.

<https://hdl.handle.net/2066/214599>

Please be advised that this information was generated on 2024-06-12 and may be subject to change.

Article 25fa End User Agreement

This publication is distributed under the terms of Article 25fa of the Dutch Copyright Act. This article entitles the maker of a short scientific work funded either wholly or partially by Dutch public funds to make that work publicly available for no consideration following a reasonable period of time after the work was first published, provided that clear reference is made to the source of the first publication of the work.

Research outputs of researchers employed by Dutch Universities that comply with the legal requirements of Article 25fa of the Dutch Copyright Act, are distributed online and free of cost or other barriers in institutional repositories. Research outputs are distributed six months after their first online publication in the original published version and with proper attribution to the source of the original publication.

You are permitted to download and use the publication for personal purposes. All rights remain with the author(s) and/or copyrights owner(s) of this work. Any use of the publication other than authorised under this licence or copyright law is prohibited.

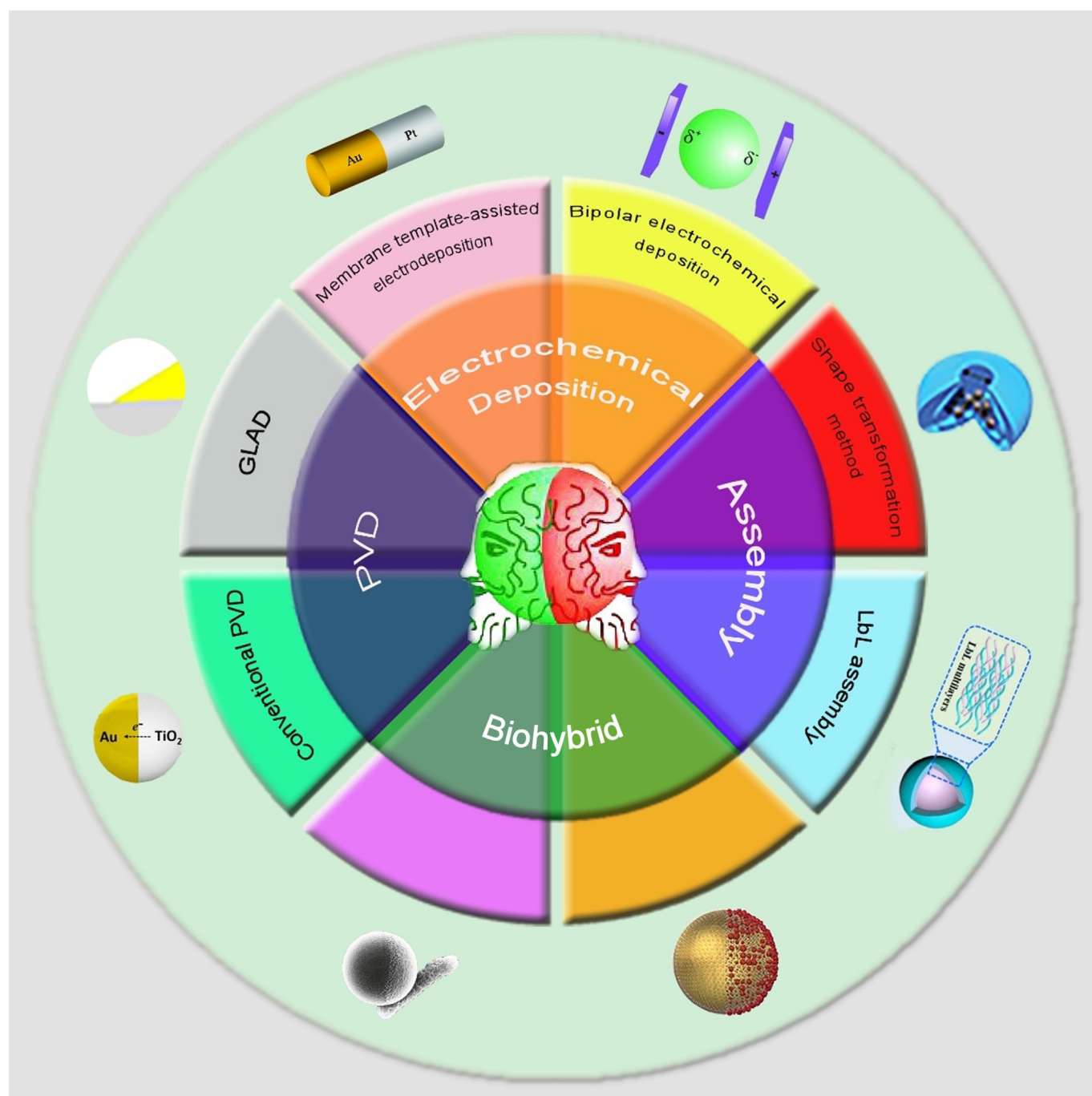
If you believe that digital publication of certain material infringes any of your rights or (privacy) interests, please let the University Library know, stating your reasons. In case of a legitimate complaint, the University Library will, as a precaution, make the material inaccessible and/or remove it from the website. Please contact the University Library through email: copyright@ubn.ru.nl. You will be contacted as soon as possible.

University Library
Radboud University

■ Synthesis Design

Fabrication of Self-Propelled Micro- and Nanomotors Based on Janus Structures

Yicheng Ye,^[a] Jiabin Luan,^[a, b] Ming Wang,^[a] Yongming Chen,^[c] Daniela A. Wilson,^[b] Fei Peng,^{*,[c]} and Yingfeng Tu^{*,[a]}



Abstract: Delicate molecular and biological motors are tiny machines capable of achieving numerous vital tasks in biological processes. To gain a deeper understanding of their mechanism of motion, researchers from multiple backgrounds have designed and fabricated artificial micro- and nanomotors. These nano-/microscale motors can self-propel in solution by exploiting different sources of energy; thus showing tremendous potential in widespread applications. As one of the most common motor systems, Janus motors

possess unique asymmetric structures and integrate different functional materials onto two sides. This review mainly focuses on the fabrication of different types of micro- and nanomotors based on Janus structures. Furthermore, some challenges still exist in the implementation of Janus motors in the biomedical field. With such common goals in mind, it is expected that the elaborate and multifunctional design of Janus motors will overcome their challenges in the near future.

1. Introduction

Biological motors can perform complicated tasks in organisms precisely after millions of years of evolution. As one of the most important biological motors, kinesins harvest energy through hydrolyzing adenosine triphosphate (ATP) to move along microtubule filaments.^[1] Inspired by nature, scientists have been designing and fabricating artificial motors, such as molecular machines, for potential applications. The 2016 Nobel Prize in Chemistry was rewarded to the study of molecular machines and this promoted the further development of molecular motors and self-propelled micro- and nanomotors. Different from molecular ones, micro- and nanomotors of larger sizes can convert chemical energy or external fields into motion. In 2002, the group of Whitesides developed the first artificial motor on the centimeter scale, which could move autonomously through the decomposition of H_2O_2 fuel.^[2] This provided a big boost for the development of catalytic micro- and nanomotors. Later, in 2004, bimetallic motors consisting of platinum and gold segments were reported upon successfully scaling down the size of motors to the micrometer level.^[3] Based on this work, various types of micro- and nanomotors were developed through either top-down or bottom-up approaches. However, the motion of motor systems in most reports was based on the platinum/ H_2O_2 reaction, which was not biocompatible for biomedical applications. To obviate the dependence on non-biocompatible H_2O_2 fuel, enzymes such as glucose oxidase (GOx) and catalase were introduced into the motor systems to achieve motion through an enzyme-based cascade reaction; thus holding great promise for biomedical fields.^[4] In addition to endogenous glucose for chemical fuel,

even water can be used for the propulsion of micro- and nanomotors.^[5] By incorporating stimuli-responsive components, these micro- and nanomotors showed considerable potential in biomedical applications because they could adapt to the complex environment.^[6] Benefitting from enhanced motion manipulation in the past decade,^[7] motor systems can act as tiny robots that make it possible to perform specific tasks inside our body.

As one of the most common motor systems, Janus motors are based on Janus particles, which are asymmetric structures with different physical or chemical properties. In 1991, de Gennes mentioned “Janus” in his Nobel lecture to define particles with two diverse hemispheres.^[8] The design and fabrication of Janus particles have been a challenge in the past ten years. From the materials perspective, there are mainly three kinds of Janus particles: polymeric, inorganic, and hybrid polymeric-inorganic; all of which possess different kinds of shapes. Due to the unique asymmetric structures of Janus particles, they are widely used for the fabrication of micro- and nanomotors. This review mainly focuses on the synthesis of micro- and nanomotors based on Janus structures. The most typical types are spherical or cylindrical Janus motors. Symmetrical tubular motors are not included herein, except for those that are conical in shape. By summarizing methods for the fabrication of Janus micro- and nanomotors, we expect to stimulate interest and encourage more research towards novel motor systems, as well as their future biomedical applications.

2. Fabrication

Herein, we introduce four different fabrication methods for the preparation of Janus motors and discuss representative examples in detail (Table 1). The shape, material, and size all contribute to the specific functions of Janus motors because the aim of fabrication is to design functional Janus motors for practical applications.


2.1. PVD

As a deposition method, PVD is used for depositing thin films and coating the surface of substrates. Through physical approaches, such as high-temperature vacuum, a solid or liquid surface of the target material is vaporized into gas-phase molecules or partially ionized into ions. A film is then formed on

[a] Y. Ye, J. Luan, M. Wang, Prof. Y. Tu
School of Pharmaceutical Science
Guangdong Provincial Key Laboratory of New Drug
Screening Southern Medical University, Guangzhou 510515 (P.R. China)
E-mail: tuyingfeng1@smu.edu.cn

[b] J. Luan, Prof. D. A. Wilson
Institute for Molecules and Materials
Radboud University of Nijmegen, Nijmegen, 6525 AJ (The Netherlands)

[c] Prof. Y. Chen, Prof. F. Peng
School of Materials Science and Engineering
Sun Yat-Sen University, Guangzhou 510275 (P.R. China)
E-mail: pengf26@mail.sysu.edu.cn

 The ORCID identification number(s) for the author(s) of this article can be found under: <https://doi.org/10.1002/chem.201900840>.

the surface of a well-arranged substrate by a low-pressure gas (or plasma). There are two common processes of PVD, namely, vacuum sputtering and vacuum ion plating. The basic principle of vacuum sputtering is to use ionized gas to form a vapor by bombarding the target material. For vacuum ion plating, an electron beam or magnetron is employed to ionize neutral particles into ions and electrons. If the substrate has an added negative bias, ions are deposited onto the surface of the substrate to form thin films. The ultimate goal of both methods is to deposit a thin layer on the semiexterior of the substance; thus introducing different properties to the two surfaces. In the following sections, we mainly introduce conventional PVD and GLAD.

2.1.1. Conventional PVD

Conventional PVD has a wide range of applications, from coating industrial products for protection to fabricating Janus particles. PVD has many advantages. First, it can deposit multifarious inorganic components and some kinds of organic materials. In addition, it is more environmentally friendly than other techniques, such as electroplating. The most important benefit is that PVD makes it easy to integrate catalytic or magnetic properties with Janus particles, which is required for the formation of micro- and nanomotors.

2.1.1.1. Spherical Janus motors

Conventional PVD is the most common method to fabricate spherical Janus motors. As the substrate spreads out onto the pretreated surfaces to form a monolayer, a thin layer of targeted materials is deposited onto the upper hemisphere of the substrate. Therefore, an asymmetrical structure can be realized easily through element deposition. For catalytic Janus micro- and nanomotors, the most widely used material is platinum. Platinum was deposited onto silica microparticles and the resulting Janus micromotors could be guided by low-height topographic steps.^[49] In a well-like structure, they could bypass the corner, but fail to switch their directional motion at the 270° corner in the post-like structure. On/off switching of the guiding of micromotors may be realized through the new design of chemically patterned walls. Similarly, Pt–SiO₂ Janus motors were demonstrated to be capable of propulsion in a crowded and confined environment, similar to that in biosystems.^[50] This special experimental setup inspired the design of novel motors to perform diverse tasks. For example, silica colloids sputtered with Ti and Pt could aggregate and passively power larger engineered objects, such as microgears.^[51] For precisely controlled motion, self-propelled bimetallic Janus micromotors were also designed.^[9] SiO₂ was first coated with Ni, followed by a thin layer of Pt deposition. The formed micromotors could be propelled in H₂O₂ and their direction could be manipulated by the external magnetic field. This provided the first example of micromotors, which could transport passive cargoes contactlessly with a magnetic dipole. This micromotor was further shown to have a tendency to chase the self-assembled particles without direct contact through magnetic dipole–

dipole interactions. This behavior was attributed to the deposited Ni magnetic material. In addition, the directional propulsion of Pt–SiO₂ could be achieved in designing asymmetric channels.^[52] The directed flow was identified by interactions between particles and particles within the model. The work showed robust control of the motion of micromotors through breaking temporal and spatial symmetry.

In addition to common catalytic Pt–SiO₂ Janus motors, there are also numerous materials that can be incorporated to fabricate multifunctional Janus motors. TiO₂/Pt Janus micromotors with in-place assembly and dissociation with precise control were presented.^[10] The TiO₂/Pt Janus micromotors were obtained by sputtering platinum on TiO₂ microspheres, which could be controlled by light. By regulating the UV-light intensity, the resulting motors could induce the assembly of dynamic colloidal particles (Figure 1A). If the UV light was turned off, the colloidal particles separated naturally due to the disappearance of the interaction. This work inspired the design of micro-

Yicheng Ye received his B.Sc. degree in pharmacy from Southern Medical University, P.R. China, in 2018. He is currently a Master's student in the School of Pharmaceutical Science at the same university. His research interests concern the construction of novel drug-delivery systems based on micro- and nanomotors.



Fei Peng received her Ph.D. (09.2013–03.2017) degree from the Institute for Molecules and Materials (IMM) with Prof. Jan C. M. van Hest and Prof. Daniela A. Wilson, Radboud University of Nijmegen, The Netherlands. After a postdoctoral position at the IMM, she joined Sun Yat-Sen University as Associate Professor (10.2017). Her group's focus is on the development of polymeric nanomotor systems for biomedical applications, including drug delivery, immunotherapy, and stem cell therapy.



Yingfeng Tu received his Master's degree in pharmaceutical science from Peking University in 2013 and his Ph.D. degree from the Radboud University of Nijmegen, The Netherlands, in the groups of Prof. Daniela A. Wilson and Prof. Jan C. M. van Hest. After a short research associate training, he was appointed Professor in the School of Pharmaceutical Science, Southern Medical University, heading the group of Nanomedicine. His current focus is on the design of intelligent self-propelled nanomotors as next-generation drug-delivery systems.

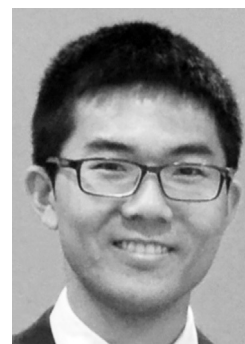


Table 1. Fabrication methods for different shapes, materials, and sizes of Janus micro- and nanomotors.^[a]

Fabrication	Shape	Material	Size [μm] ^[b]	Propulsion mechanism	Motion control	Ref.		
PVD	conventional PVD	SiO ₂ /Ni/Pt	Φ 2.2	bubble propulsion	magnetic field	[9]		
		TiO ₂ /Pt	Φ 1.2	self-electrophoresis	UV light	[10]		
		SiO ₂ /Ir	Φ 1.2	self-diffusiophoresis	magnetic field	[11]		
		Al–Ga/Ti	Φ 20	bubble propulsion	n.a.	[5]		
		Mg/ZnO, Zn/Fe	Φ 30	bubble propulsion	n.a.	[12]		
		Mg/Au	Φ 20	bubble propulsion	n.a.	[6, 13]		
		Mg/Ag	Φ 20	bubble propulsion	n.a.	[14]		
		Mg–Fe/Au	Φ 15 \pm 5	bubble propulsion	magnetic field	[15]		
		SiO ₂ /Au	Φ 5	self-diffusiophoresis	NIR light	[16]		
		TiO ₂ /Au	Φ 1	self-electrophoresis	UV light	[17]		
		Cu ₂ O/Au	Φ 1.2	self-electrophoresis	visible light	[18]		
		BiOI/Au	Φ 2–4	self-electrophoresis	visible light	[19]		
		TiO ₂ /Fe	Φ 2	self-electrophoresis	magnetic field	[20]		
		GLAD	dumbbell rod	silica/Pt–SiO ₂	Φ 0.2–0.97	self-diffusiophoresis	n.a.	[21]
				Pt–SiO ₂	L 2.6; Φ 0.63	self-electrophoresis	n.a.	[22]
			Pt–SiO ₂ t	Φ 2.59	bubble propulsion	n.a.	[23]	
	sphere		silica/Au/Pt	Φ 2.01	self-electrophoresis	n.a.	[24]	
			Au/Pt	Φ 0.03	self-electrophoresis	n.a.	[25]	
	electrochemical deposition		virus/Pt	Φ 0.025–0.03	self-diffusiophoresis	n.a.	[26]	
			TiO ₂ /Au/Pt	Φ 1.2	self-electrophoresis	UV light	[27]	
		PS beads and Ni nano-rods	Φ 0.5; L 1	magnetic actuation	magnetic field	[28]		
rod		Si/Pt, Si/Ag	L 3.0; W 0.35	bubble propulsion	n.a.	[29]		
tadpole		TiO ₂ /silica/Pt	L 3.5; Φ 2.01	bubble propulsion	n.a.	[30]		
			L 6; Φ 2.01					
spiral		silica/Co	L 1–2; W 0.2–0.3	magnetic actuation	magnetic field	[31]		
membrane template-assisted deposition			Pt/Au	L 2; Φ 0.37	self-electrophoresis	n.a.	[3]	
			Ni/Au	L 2.5; Φ 0.2	self-electrophoresis	n.a.	[32]	
			Pt/Au	L 5; Φ 0.25	self-electrophoresis	electric field	[33]	
		Au/Ag/Ni	L 6.5; Φ 0.2	magnetic actuation	magnetic field	[34]		
		Au/Fe ₂ O ₃	L 6; Φ 0.3	self-electrophoresis	magnetic field	[35]		
bipolar electrochemical deposition		Au/Ru/Ni	L 2.03; Φ 0.3	acoustic actuation	magnetic field	[36]		
	tube	Au/Pt	L 4.5; Φ 0.3	bubble propulsion	n.a.	[37]		
		carbon microtube/Pt	L 5–20	bubble propulsion	n.a.	[38]		
	tube	carbon tube/Ni	L 20	magnetic attraction	magnetic field	[39]		
	others	polyaniline/alginate	n.a.	bipolar electro-chemistry	n.a.	[40]		
assembly	shape transformation method	stomatocytes	PEG-PS	Φ 0.32	bubble propulsion	n.a.	[41]	
				Φ 0.22	light actuation	NIR light	[42]	
	LbL assembly	capsule	PSS-PAH/SiO ₂ -Pt	Φ 8	bubble propulsion	magnetic field	[43]	
biohybrid	cluster				NIR light	[44]		
					magnetic field	[45]		
	sphere		mesoporous silica/Ni/catalase	Φ 0.1	bubble propulsion			
		PLL-g-PEG-cat/GOx	Φ 0.8	self-diffusiophoresis	n.a.	[46]		
		mesoporous silica-urease	Φ 2.32	chemophoretic	n.a.	[47]		
		PS/Pt– <i>E. coli</i>	Φ 2	n.a.	n.a.	[48]		

[a] PVD = physical vapor deposition, GLAD = glancing angle deposition, LbL = layer-by-layer, n.a. = not available, NIR = near-infrared, PS = polystyrene, PEG = polyethylene glycol, PSS = polystyrene sulfonate, PAH = polyallylamine hydrochloride, PLL-g-PEG = poly(L-lysine)-graft-poly(ethylene glycol). [b] Φ = diameter, L = length, W = width.

[a] PVD = physical vapor deposition, GLAD = glancing angle deposition, LbL = layer-by-layer, n.a. = not available, NIR = near-infrared, PS = polystyrene, PEG = polyethylene glycol, PSS = polystyrene sulfonate, PAH = polyallylamine hydrochloride, PLL-g-PEG = poly(L-lysine)-*graft*-poly(ethylene glycol). [b] Φ = diameter, L = length, W = width.

motors with controllable and reversible motion behavior. combining catalytic and magnetic actuation.^[53] Thin layers of Open-loop control of micromotors can also be achieved by Ni and Pt were sequentially deposited on predried silica micro-

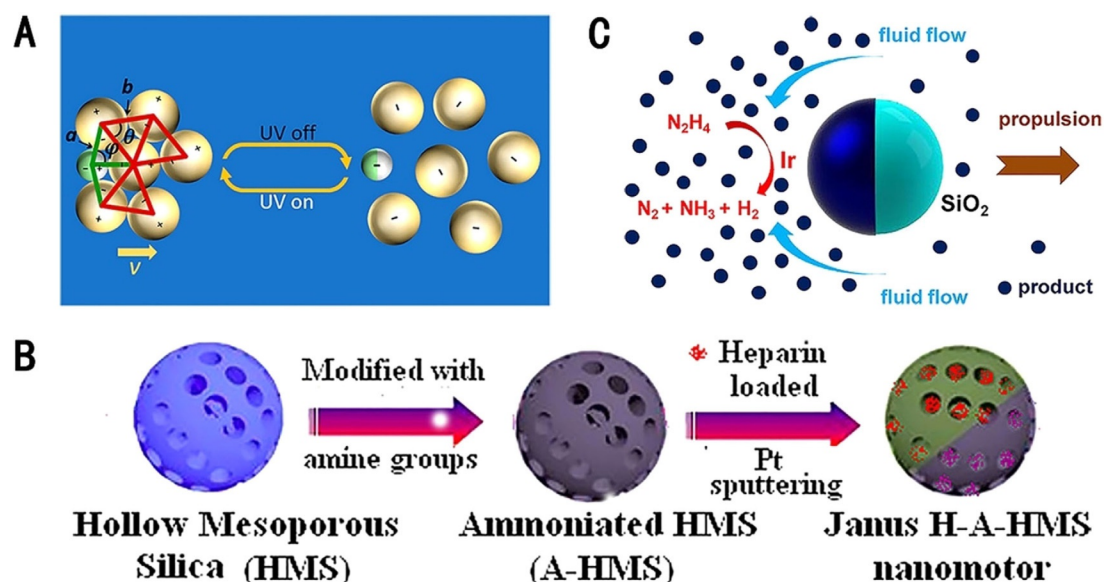


Figure 1. Conventional PVD of spherical Janus motors. A) UV-light-controlled Janus TiO_2/Pt micromotors. Reprinted with permission from ref. [10]. Copyright 2017 American Chemical Society. B) Heparin-loaded Janus nanomotors. Reprinted with permission from ref. [55]. Copyright 2018 American Chemical Society. C) Ir-SiO₂ micromotors propelled in ultralow levels of hydrazine. Reproduced with permission from ref. [11]. Copyright 2014 American Chemical Society.

particles by means of electron-beam deposition to prepare the Janus micromotors.^[54] These Janus micromotors could be precisely controlled to perform presupposed tasks under external electric and magnetic fields, without the use of any harmful chemical fuels; thus showing promise for biomedical applications. To achieve drug loading, HMS nanoparticles (NPs) were used (Figure 1B).^[55] The mesoporous silica NPs were first modified chemically with amine groups followed by a heparin-loading process. Then a thin layer of platinum was deposited on one side by sputtering to obtain Janus nanomotors. These Janus nanomotors could be propelled and had excellent blood compatibility.

For catalytic micro- and nanomotors, the speed of the motors hinged upon the concentration of the fuel. In general, power generated by the catalytic reaction of a low concentration of fuel was not sufficient for their movement to overcome resistance from the viscosity of the solution or Brownian motion of NPs. Therefore, scientists have employed different materials in PVD to fabricate versatile micro- and nanomotors. Iridium-based Janus micromotors were reported to be propelled at high speed in ultralow levels of hydrazine fuel solution (Figure 1C).^[11] Janus micromotors were fabricated through deposition of a thin layer of iridium on silica microparticles. For catalytic micromotors, this was the first time that hydrazine had been utilized as a fuel. Compared with traditional platinum-based micromotors, catalytic iridium motors displayed considerable speed, over $20 \mu\text{m s}^{-1}$, while consuming fuel at a lower concentration of less than 10000-fold because of osmotic effects.

To expand the extensive applications of micro- and nanomotors in the biomedical field, the choice of fuel is of great significance. Widely used H_2O_2 fuel, which is harmful to biological systems, hinders the application of motors in biological media. The first water-driven micromotor was demonstrated by de-

composing water into hydrogen bubbles (Figure 2A).^[5] The micromotor was composed of Al–Ga alloy and Ti was coated on the hemisphere through electron-beam evaporation. This efficient micromotor showed fast speeds in media of both water and human serum. The power could be derived from acidic to alkaline solutions, since it is well known that Al has an amphoteric performance. Additionally, the speed of the micromotor decreased with increasing salt concentration because high ionic strength resulted in larger bubble sizes and fewer bubbles. Because the active metal possesses remarkable properties such as biocompatible and environmentally friendliness, it is an ideal material for the fabrication of Janus micro- and nanomotors. Due to the reaction between Mg and water, Janus micromotors with controllable degradation were demonstrated (Figure 2B).^[12] The Mg microparticles were spread in a monolayer on the glass slide. ZnO was coated on the exposed part of the particles through electron-beam evaporation, resulting in low exposure of Mg for the reaction with water. At the same time, the Zn/Fe Janus micromotors were fabricated by means of Fe deposition on the hemisphere of Zn microparticles.^[12] This kind of self-destroyed micromotor exhibited efficient motion and controlled degradation in biological fluid. Based on Mg microparticles, Au was coated on one side of the microparticles by using an electron-beam evaporator.^[13a] The Au surface was further modified with DMSA, which exhibited high efficiency for the elimination of toxic heavy-metal ions (Figure 2C). Additionally, diphenyl phthalate could also be detected sensitively with the same Mg/Au Janus micromotors.^[13b]

To endow the Mg/Au Janus micromotor with more functions, they could also be coated with a pH-sensitive drug-loaded polymeric layer.^[6] These Janus micromotors were demonstrated to safely and quickly deplete excess gastric acid and release drugs. Mg/Ag Janus micromotors showed much better antibacterial properties compared with those of static Janus

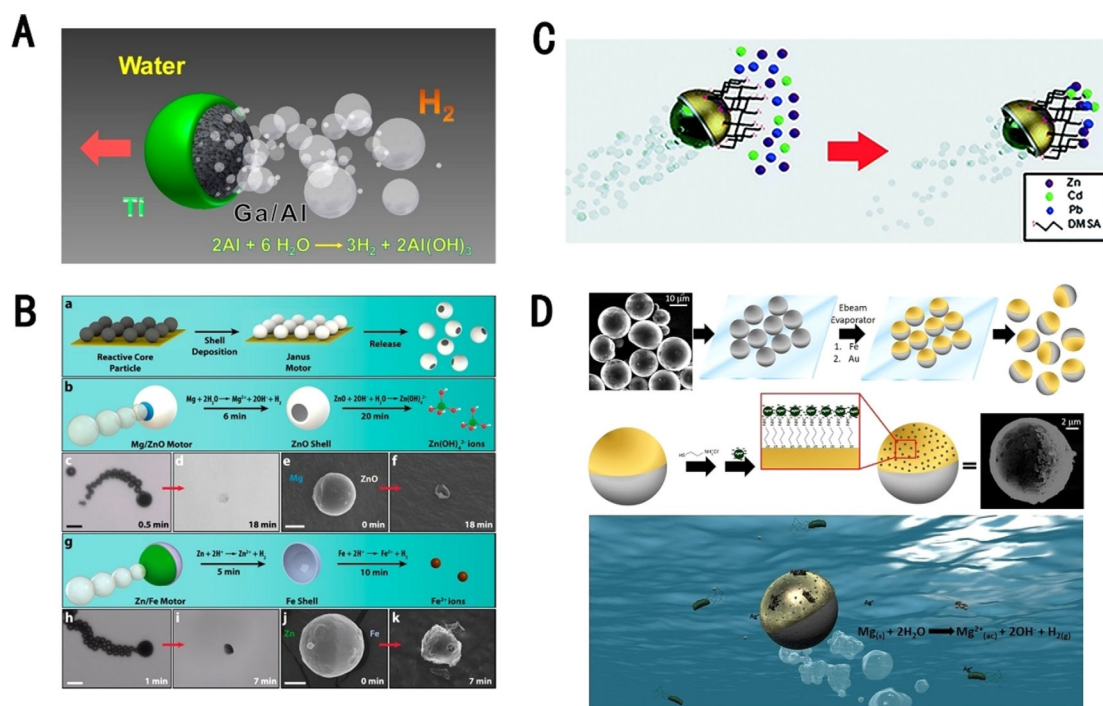


Figure 2. Conventional PVD of spherical Janus motors. A) A water-driven hydrogen-propelled Al–Ga/Ti micromotor. Reprinted with permission from ref. [5]. Copyright 2012 American Chemical Society. B) Fabrication of transient micromotors and their motion and degradation processes. Reproduced with permission from ref. [12]. Copyright 2016 American Chemical Society. C) Janus micromotor for the removal of toxic metals. DMSA = *meso*-2,3-dimercaptosuccinic acid. Reproduced with permission from ref. [13a]. Copyright 2016 Royal Society of Chemistry. D) Fabrication of a water-propelled Janus micromotor and modification with Ag NPs for bactericidal action. Reproduced with permission from ref. [15]. Copyright 2017 American Chemical Society.

particles.^[14] A multifunctional Mg-based micromotor with various metal layers was also described (Figure 2D).^[15] Janus structures based on spherical Mg microparticles were achieved by depositing metal caps of Fe and Au. Ag NPs with antibacterial properties were conjugated onto the surface of the Au layer afterwards. This type of Janus micromotor could be propelled through an aqueous solution and showed high efficiency in killing bacteria. With a magnetic Fe layer, the micromotors could be controlled by means of an external magnetic field. During the Mg–water reaction, a passivation layer formed on the Mg surface, which hindered the reaction. Compared with individual Mg particles, Janus bimetallic motors prevented the formation of a passivation layer, which was propitious in allowing smooth propulsion.

In addition to chemically propelled motors, there are also numerous fuel-free motors. In addition to Mg being employed to design micro- and nanomotors, Au also plays a significant role in the fabrication of motors due to its easy modification and excellent photothermal effect. Au–SiO₂ Janus micromotors have been studied widely.^[16,56] In general, SiO₂ microparticles were dispersed on the pretreated wafer to form a monolayer and dried under vacuum. The Au layer was half-coated through conventional PVD, followed by ultrasonic treatment and centrifugation. The force generated by self-thermophoretically driven Au–SiO₂ Janus particles could stretch individual double-stranded DNA molecules.^[56c] Furthermore, the synergistic effect of self-thermophoresis and active targeting of cancer cells by coating the macrophage cell membrane (MPCM) on

the Au–SiO₂ Janus nanomotors was reported (Figure 3A).^[16] After light illumination, the nanomotor could perforate the cytomembranes through a photothermal effect. This multifunctional self-propelled nanomotor showed potential for in vivo applications.

TiO₂ is an ideal photocatalytic material that has good physical and chemical properties.^[17,57] Similar to previous reports, a monolayer of TiO₂ microparticles was prepared followed by coating with Ni and Au through conventional PVD. The as-formed Janus micromotors could be propelled efficiently under a low intensity of UV light. By modulating the light intensity, control over the speed of the Janus micromotors was achieved (Figure 3B).^[17] By implanting a magnetic layer of Ni, the direction of the micromotors could be precisely controlled.^[57b,58] Because UV light is harmful to living organisms, efforts still need to be made to develop a substitute for UV light. Fortunately, multiwavelength light-actuated Janus micromotors were presented (Figure 3C).^[57c] A layer of Au was half-deposited on the self-assembled black TiO₂ (B-TiO₂) microspheres. The motion of this Janus micromotor could be activated by a wide range of light absorption from $\lambda = 300$ to 800 nm; thus suggesting a potential employment of solar energy. A type of visible-light-propelled Janus Cu₂O–Au micromotors with “ON–OFF” motion and controlled motion behavior was also demonstrated.^[18] The Cu₂O microspheres were coated with an Au layer through thermal evaporation. Furthermore, due to the excellent photocatalytic activity against pure water, bismuth oxyiodide (BiOI)-based Janus micromotors could be propelled

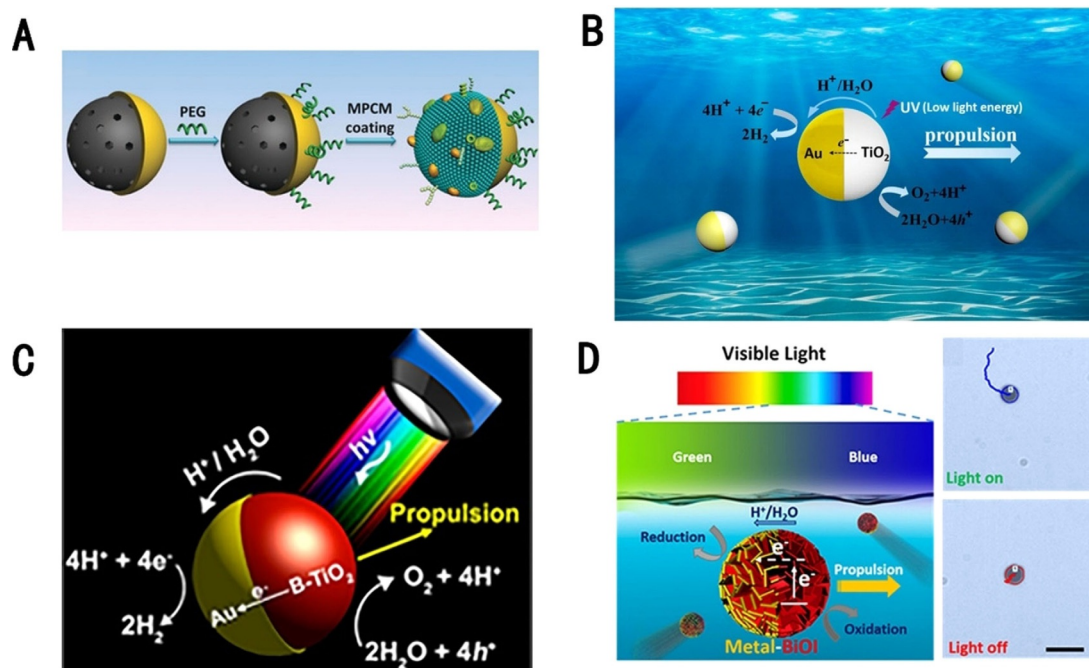


Figure 3. Conventional PVD of spherical Janus motors. A) Schematic illustration of the fabrication of a MPCM cloaking a Janus nanomotor. Reproduced with permission from ref. [16]. Copyright 2018 Wiley-VCH. B) Schematic illustration of a UV-light-powered TiO_2/Au Janus micromotor. Reproduced with permission from ref. [17]. Copyright 2016 American Chemical Society. C) Schematic illustration of multiwavelength light-actuated Janus micromotors. Reproduced with permission from ref. [57c]. Copyright 2017 American Chemical Society. D) Schematic illustration of visible-light-propelled and -controlled motion of a Janus micromotor. Reproduced with permission from ref. [19]. Copyright 2017 American Chemical Society.

by visible light (Figure 3D).^[19] A thin Au layer was deposited onto the hemisphere of the BiOI microspheres by means of sputter coating. A magnetic field is another attractive strategy to control motion through the incorporation of magnetic materials. Generally speaking, magnetic control is a harmless approach to control motion efficiently and effectively. Magnetically powered Janus micromotors obtained by depositing a layer of Ni onto SiO_2 were demonstrated.^[59] The deposition of magnetic Fe was also used to control the direction of micro- and nanomotors.^[20] Therefore, a magnetic field not only provides power for the movement of the motors, but also guides their direction.

2.1.1.2. Other shapes

In addition to spherical Janus motors, PVD is also used to fabricate many other shapes of Janus motors. A dumbbell-like Janus nanomotor, composed of a catalytic platinum sphere connected to noncatalytic silica beads, was presented.^[21] The sub-monolayer of silica microbeads was prepared before coating with Cr and Pt through sputtering. The thin layer of Cr was used to improve adhesion between silica microbeads and the thicker Pt layer. The metallic half-shell shrank into a Pt particle and attached to the silica beads during thermal annealing. The velocity of the motors was affected by the diameter ratio of Pt to silica particles. Rod-shaped Janus micromotors are also attractive. Side-propelling Janus rods with different aspect ratios were developed.^[22] The silica rods lay horizontally to form a monolayer on clean glass. Then a thin layer of Pt was vertically

deposited on top of the rods. To avoid the undesired formation of bubbles, a low concentration of H_2O_2 was employed. This work systematically explored the internal propulsion mechanism and dynamic self-organization of motors.

2.1.2. GLAD

Due to the limited functional diversity of single surface deposition, researchers proposed GLAD. GLAD, or dynamic shadowing growth, is one of the PVD methods with which the position of a substrate is variable during the deposition process or the vapor is deposited at a flexible angle relative to the vertical direction used in conventional PVD. The substrate is generally immobilized on the wafer and adjusted at a tilted angle to the vapor flux to obtain particles of different geometries. The target can be deposited with multiple size scales of different materials by changing the angle between the substrate and evaporator source during deposition. The thickness of the deposited layer and geometric structures can be controlled by adjusting the vapor rate and rotating the substrate.

2.1.2.1. Spherical Janus motors

Janus micro- and nanomotors fabricated by means of GLAD can be endowed with novel properties and capabilities. Self-propelled Janus micromotors were reported through the deposition of a thin Pt layer on silica microparticles at a small angle (Figure 4A).^[23] The resulting micromotors were further modified with biotin, which could pick up and transport charged or

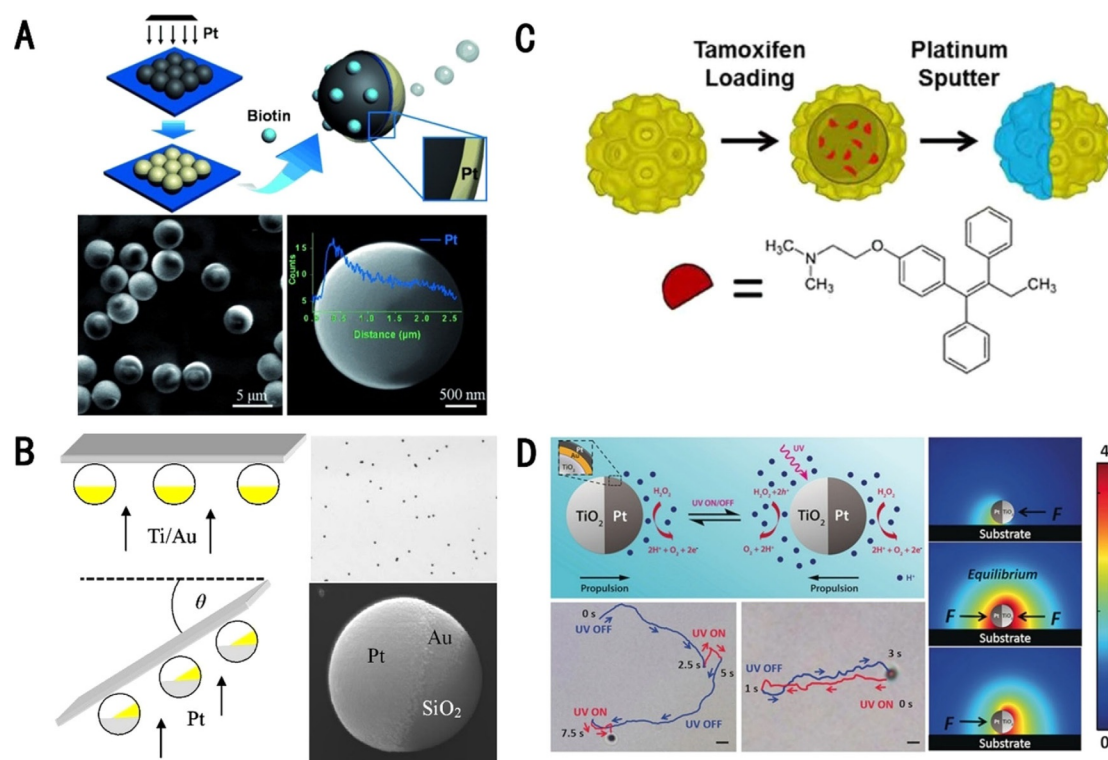


Figure 4. GLAD of spherical Janus motors. A) Preparation of a biotin-modified Janus micromotor. Reproduced with permission from ref. [23]. Copyright 2015 Wiley-VCH. B) Schematic illustration of the preparation of a SiO₂/Au/Pt micromotor, with the corresponding SEM image. Reproduced with permission from ref. [24]. Copyright 2010 American Institute of Physics. C) Preparation of a virus-based Janus nanomotor for cargo delivery. Reproduced with permission from ref. [26]. Copyright 2019 Wiley-VCH. D) Mechanism of optical brakes on a TiO₂/Au/Pt Janus micromotor. Reproduced with permission from ref. [27]. Copyright 2018 Wiley-VCH.

ganic dyes selectively, while maintaining a fast speed. Asymmetric spherical Janus micromotors prepared through dynamic shadowing growth were also developed (Figure 4B).^[24] Bi-metallic Ti and Au were sequentially deposited on the surface of the silica microbeads, while the substrate was rotated at a polar angle at the same time. By adjusting the angle of rotation, a thin layer of Pt was coated on the substrate to form an exposed part of the Au layer, which was difficult to achieve by means of conventional PVD. Compared with micromotors without the Au layer, the speed of the Pt/Au micromotor increased with an increase of the exposed Au area; this was attributed to a self-electrophoresis mechanism. Similarly, Pt/Au Janus nanomotors, with sizes of 30 nm, were also fabricated; these were the smallest nanomotors at that time.^[25] Through block copolymer micelle lithography, Pt served as a nanoseed and rotated as Au was deposited by means of GLAD. This nanomotor was able to move efficiently in solution, regardless of strong Brownian motion due to its small size. Furthermore, polymeric vesicles deposited with Pt showed a high drug-loading efficiency.^[60] The obtained Janus motors showed enhanced permeation and retention effects across the endothelium. The virus capsid was also used for the fabrication of micro- and nanomotors (Figure 4C).^[26] A thin layer of Pt was deposited on one hemisphere of capsids from a plant virus. Because the tumor sites produce a high concentration of H₂O₂ and lower pH, the virus-based nanomotors showed an ability to target to specific areas and release the drug under pH stimuli. The capsid carri-

ers showed enormous advantages compared with those of other materials, such as great biocompatibility and safety, as well as a high loading capacity. Surface modification was also easy to achieve in this system to target specific tissues actively. Therefore, virus-based nanomotors provided new possibilities in biomedical applications.

Precise control and manipulation of the motion of micro- and nanomotors is the other demanding difficulty to overcome. The first chemical-/light-powered micromotors with built-in optical brakes were reported recently (Figure 4D).^[27] The micromotors were composed of photocatalytic TiO₂ and catalytic Pt. The TiO₂ microparticles were dispersed into a monolayer on glass slides, followed by the deposition of an Au layer at an angle to TiO₂ rotation. Catalytic Pt was deposited in the same way without rotating substrates, which resulted in a partially exposed Au layer. The micromotors were propelled by self-electrophoresis through the chemical catalysis of Pt. Photocatalytic TiO₂ could be used to switch or reverse the direction of movement under light stimulus. These micromotors integrated two independent propulsion modes and encouraged more intellectualized design of controllable micro- and nanomachines.

2.1.2.2. Other shapes

In the design of catalytic micro- and nanomotors, GLAD offers possibilities to fabricate a wide range of novel and complex

structures. By changing the vapor direction and substrate rotation, multifunctional materials can be grown as a single particle to achieve diverse motion. Apart from spherical Janus motors, GLAD has also been employed to fabricate many other Janus motors with different shapes. In the fabrication of tadpole-like nanomotors, silicon microbeads were immobilized onto wafers, spread to form a monolayer, and rotated at a tilted angle. Then the TiO_2 nanoarms were deposited through dynamic shadowing growth (Figure 5A).^[30] Subsequently, the substrates were set back to the horizontal position and rotated while the Pt layer was deposited. Because the nanoarms were attached obliquely to silicon, asymmetric structures were introduced through the deposition of Pt at one end of the TiO_2 nanoarm. The tadpole-like nanomotors formed exhibited a rotating motion in H_2O_2 . Four different kinds of nanorods were also developed by the same group.^[29] The rotary Si/Pt and Si/Ag nanorods were fabricated by means of GLAD to form the Si nanorod backbones, followed by deposition of Pt or Ag layers, respectively, on one part of the nanorod to induce asymmetric structures. The L-shaped Si/Pt nanorods were composed of two arms of different lengths (Figure 5B). One shorter Si arm was fabricated by the same method as that described previously, and the substrate was azimuthally rotated quite quickly before deposition of the other longer Si arm. Finally, the symmetric structure was broken by coating a thin layer of Pt on the surface of the longer nanorod with the substrate tilted at a small angle. Ag was also employed as the catalyst. The L-shaped Si/Ag nanorod was prepared by depositing Ag on one end of both the short and long nanorods through a similar process. The complex structure of a Si/Ag nanospring was also achieved by adjusting the deposition angle and substrate rotation. V-shaped nanomotors based on TiO_2 employing Ni can be used for magnetic actuation. The first TiO_2 arm was deposited at an angle by means of dynamic shadowing growth, followed

by deposition of a Ni layer on the end. After rapid rotation, the other layer of Ni was deposited, followed by the growth of a second TiO_2 arm. The substrate was then rotated at a different azimuth, and a Pt layer was deposited at an angle on one arm, producing the asymmetric distribution of the catalyst. Both hemispherical microbeads with Ni coating and V-shaped arms were magnetized and mixed together; shaking induced self-assembly into the V-shaped nanomotor. A rod-shaped magnetic nanomotor with Ni coating on the monolayer of PS beads was fabricated by means of GLAD (Figure 5C).^[28] Nickel rods were grown on the surface of PS beads at a vapor incident angle, with a quartz crystal microbalance to monitor the deposition length. These examples show the potential of GLAD for the design of complex shapes and may stimulate increasing interest in the fabrication of micro- and nanomotors with elaborate structures in the future.

Through coating functional materials such as catalytic and magnetic metals by means of GLAD, the superior properties of polymers and inorganic Janus particles can be integrated. In helical nanostructures, oblique vapor of SiO_2 was deposited on rotating PS beads through GLAD and then coated with ferromagnetic cobalt.^[31] The formed nanopropellers could be driven precisely through water by a homogeneous magnetic field. Other magnetic actuation nanopropellers of a smaller size were reported; Ni was half-coated on SiO_2 before deposition of silica helices through GLAD.^[62] The resulting helical motors, with a filament diameter of around 70 nm, were able to move through viscoelastic hyaluronan gels, and thus, were promising for biological applications.

To realize the motion of micro- and nanomotors in biological tissues, researchers have invested much effort. Among which, helical magnetic micropropellers prepared through GLAD were shown to be capable of penetrating the vitreous body and reaching the retina (Figure 5D).^[61] Nickel was deposited onto

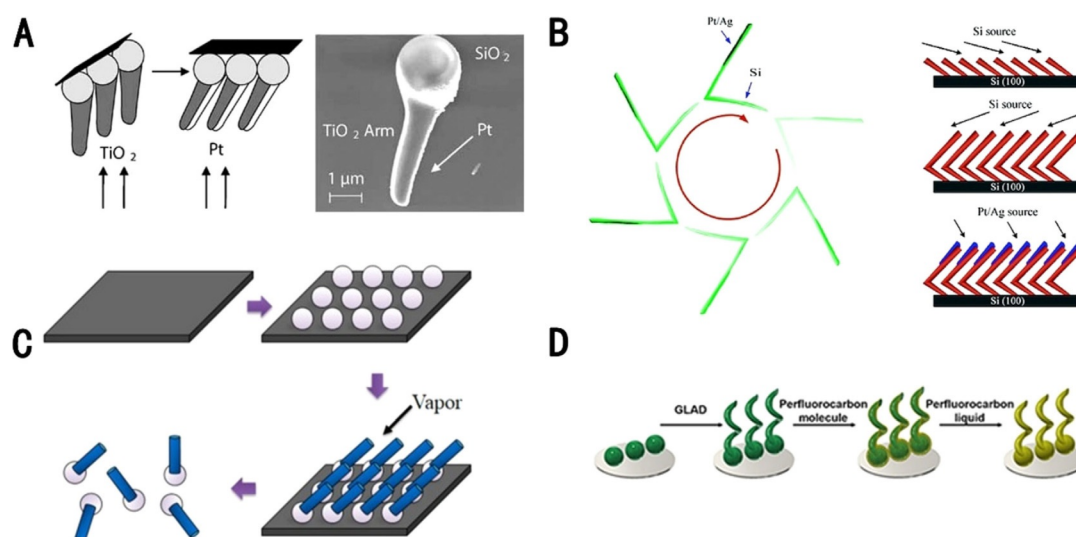


Figure 5. GLAD of other Janus motors. A) Synthesis of tadpole-like nanomotors, with the corresponding SEM image. Reproduced with permission from ref. [30b]. Copyright 2010 Wiley-VCH. B) Schematic illustration for the preparation procedure of L-shaped nanomotors. Reproduced with permission from ref. [29]. Copyright 2007 American Chemical Society. C) Preparation of rod-shaped nanomotors by means of GLAD. Reproduced with permission from ref. [28]. Copyright 2014 American Chemical Society. D) The fabrication process for perfluorocarbon-coated "slippery" micropropellers. Reproduced with permission from ref. [61]. Copyright 2018 Science Publishing Group.

silica particles at a specific incidence angle. Then silica was sequentially deposited upon rotation of the substrate to form a helical structure. The micropropellers were then coated with slippery perfluorocarbon to reduce adhesion, and they were small enough to pass through the vitreous humor in the presence of a rotating magnetic field.

2.2. Electrochemical deposition

Electrochemical deposition utilizes oxidation and reduction or an external electrical current to deposit metallic, organic, or inorganic materials on the substrate for the purpose of protecting the surface from corrosion with superior performance. It has been extensively used in the manufacturing of various products used in our daily life. Compared with PVD, electrochemical deposition is a more convenient, low-cost technique for the fabrication of structures with controllable and different dimensions. Therefore, it is not only used for coating a variety of substrates, but also for fabricating micro- and nanomotors of different shapes.

2.2.1. Membrane template-assisted electrodeposition

Membrane template-assisted electrodeposition and its derivatives have been developed recently. A variety of nanostructures with different components, such as magnetic materials, metals, alloys, semiconductors, and conductive polymers, have been successfully fabricated by using this technique.^[63] Membrane template-assisted electrodeposition employs materials with nanopores as cathodes. The nanopores act as a reaction cell, in which the material is directed by electrochemical reduction at the cathode. The walls of the pores from the templates shape the deposited materials, producing the specific structure of nanomotors. The most frequently used membranes are porous aluminum oxide and polycarbonate templates. Uniform pores of the template contribute to the mass production of nanomotors with similar structures. More importantly, the diameter and length of the rod-shaped motors can be adjusted by tuning the pore diameter and current intensity. With simple equipment and low costs, monodisperse nanomotors with different sizes and shapes can be easily obtained from multiple materials.

2.2.1.1. Cylindrical Janus motors

Various metal nanostructures, including asymmetric striped particles, were prepared through membrane template-assisted electrodeposition more than 20 years ago.^[64] Electrochemical reduction was carried out to form the desired shape in the pores of membrane templates. Various kinds of metals could be fabricated into discernible miniaturized stripes of different lengths.^[65] These pioneering studies have attracted widespread interest and encouraged scientists to develop Janus motors in this way. For instance, a similar structure of a catalytic nanomotor with 2 μm Au and 500 nm Ni in length was synthesized.^[32] First, Au was sputtered on an alumina membrane, and a working electrode was deposited through electrodeposition of Au

into the nanosized pores of the template. A sacrificial segment of Cu was then deposited, followed by the deposition of Ni and Au sections sequentially. The nanorods were obtained after dissolving the alumina membrane in a solution of sodium hydroxide and removing the sacrificial layer through chemical etching. Other Pt/Au nanorods of 370 nm in diameter and 1 μm Pt and 1 μm Au in length were synthesized by using a similar process (Figure 6A).^[3] The formed nanorods exhibited a fast speed through a solution of H_2O_2 under bubble propulsion. These nanomotors could produce an electric field that resulted in attractive and repulsive interactions.^[66] This study may inspire further studies on the interactions of motors for diverse applications. Furthermore, precise control of bimetal nanorods was achieved by electric fields.^[33] The nanomotors were aligned by the alternating current (AC) electric fields and immediately altered their speeds in the presence of direct current (DC) electric fields.

By using membrane template-assisted electrodeposition, magnetic materials can also be incorporated. Therefore, micro- and nanomotors can be driven by an external magnetic field. The first magnetically driven flexible nanowire motors were demonstrated by linking Au and Ni segments with a partially dissolved and weakened Ag bridge.^[34] Au, Ag, and Ni segments were sequentially deposited into the alumina membrane micropores. Selective and partial dissolution of the central Ag segment in H_2O_2 to create a bridge is essential for the mechanical deformation of the Ag segment, as induced by the rotation of Ni under an external rotating magnetic field. By manipulating the magnetic field, the motion of nanowires was controlled precisely. In another study, the planar fluctuation of three-link nanowires was achieved in a planar-oscillating magnetic field (Figure 6B).^[67] Motion of the Ni segment was always aligned with the orientation of an external oscillating magnetic field because of the exerting torque, which was different from the undulating motion of the Ppy tail. Through motion analysis of different nanowires, the speed increased with increasing freedom in the tail by introducing a hinge. Moreover, the gradients of applied magnetic fields could be utilized to propel a bimetallic nanomotor with the incorporation of Ni.^[68] To fabricate motors with dual motion modes, rod-shaped gold/iron oxide nanomotors activated by visible light and steered through external magnetic fields were reported (Figure 6C).^[35] A silver layer acted as a working electrode on an anodic alumina membrane, followed by electrochemical deposition of silver, gold, and iron segments in the pores and further thermal annealing. This strategy enabled the production of visible-light-driven and magnetically steerable nanomotors in an inexpensive and scalable way.

Ultrasound-propelled cylindrical motors have also been studied in depth recently. The sacrificial silver segments plated into the pores of anodic alumina membranes typically had convex tips, which resulted in the concave end of the plated metal. The second metal segment could form into flat or convex tips depending on different surface interactions with the alumina pore walls (Figure 6D).^[69] Shape anisotropy was used to explain the axial motion of bimetallic rods toward the concave end without additional chemical fuels. With increasing rod

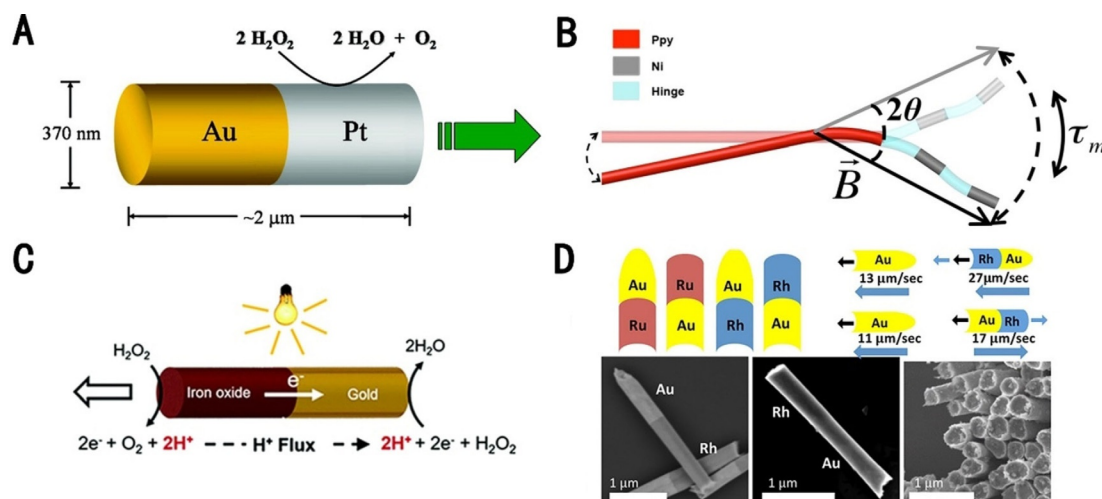


Figure 6. Membrane template-assisted electrodeposition of cylindrical Janus motors. A) Schematic illustration of the Pt (1 μm)/Au (1 μm) nanorod. Reproduced with permission from ref. [3]. Copyright 2004 American Chemical Society. B) Schematic illustration of the three-link nanomotor with undulation motion in an oscillatory magnetic field. Ppy = polypyrrole. Reproduced with permission from ref. [67]. Copyright 2015 American Chemical Society. C) The propulsion mechanism of gold/iron oxide nanomotors triggered by visible light. Reproduced with permission from ref. [35]. Copyright 2017 Royal Society of Chemistry. D) Schematic illustration of the bimetallic nanorod motors, with corresponding SEM images. Reproduced with permission from ref. [69]. Copyright 2016 American Chemical Society.

length, the speed of motion decreased. Alone in an acoustic field, the micromotors were driven along the bottom surface. Upon combining the acoustic force with chemical fuel, both positive and negative rheotaxis were achieved, which was similar to the natural behavior.^[70] Moreover, the nanorod-based motor system could spontaneously assemble into di-, tri-, and tetramers through ultrasound-induced levitation.^[36]

2.2.1.2. Tubular Janus motors

Because most chemically propelled cylindrical Janus motors move by a self-electrophoresis mechanism in solution, their motion will be undermined in a highly ionic environment and complicated biological fluids.^[71] Tubular Janus motors become favorable because they are propelled by means of bubble production. These motors possess multifunctional architectures with a functionalized outer layer and catalytic inner layer for propulsion. The first tubular micromotors were demonstrated in 2008 through a rolling-up technique.^[72] However, this technique requires a complex fabrication process and consequent costs of mass production. To overcome this drawback, membrane template-assisted electrodeposition was used as a substitute. Au–Pt bimetallic nanotubes of 300 nm in diameter and 4.5 μm in length were developed by means of electrodeposition; these nanotubes exhibited various types of movements, such as straight, screw-like, and circular motions (Figure 7A).^[37] Silver conductive ink was employed at the bottom of an aluminum oxide template, followed by the attachment of aluminum foil to act as the working electrode. Similarly, bimetallic Cu–Pt nanotubes with colloidal graphite ink were also reported.^[73] By adjusting the deposition parameters, metals can be deposited on the walls instead of in porous cavities. Catalytic Pt was grown on the inner surface of the tube. Both of these examples provide a convenient and low-cost technique to design

tubular micromotors. To increase the motor efficiency, graphene/Ag–MnO₂ micromotors were developed, which exhibited more efficient motion in a lower concentration of H₂O₂ compared with that of Pt-based micromotors (Figure 7B).^[74]

Instead of metals, conductive polymers were also incorporated into the fabrication of functional tubular motors through membrane template-assisted electrodeposition. Conducting polymer–metal tubular micromotors were synthesized through a simplified and inexpensive method (Figure 7C).^[75] Because the cyclopores of a polycarbonate membrane have a symmetrical conical structure, this is an ideal template to fabricate asymmetrical microtubes by using one portion of the double cone. The PANI film was rapidly formed on one side of the double cone through solvophobic and electrostatic effects, followed by the deposition of a Pt layer. The bilayer PANI/Pt microtubes had a significantly smaller scale compared with that of the rolled-up ones and moved at an extremely fast speed under ultralow fuel concentrations. In a similar way, conical bilayer tubular micromotors with PEDOT as the outer layer and MnO₂ as the inner layer were fabricated (Figure 7D).^[76] PEDOT was electropolymerized in a plating solution cell, followed by deposition of the MnO₂ layer. These micromotors hold great promise for application as drug-delivery vehicles, as demonstrated by the delivery of camptothecin with efficient motion and good biocompatibility. A new type of micromotor was reported based on MIPs (Figure 7E).^[77] The complementary binding sites were created through polymerization of the polymeric matrix around the analyte molecule and then removal from the print template. The tailor-made recognition sites of the micromotors could selectively bind biomolecules showing recognition properties. Meanwhile, extremely acidic media could also be used for the propulsion of polymer–metal motors (Figure 7F).^[78] The inner layer Zn of PANI/Zn microtubes was able to produce hydrogen in acidic environments, without addition-

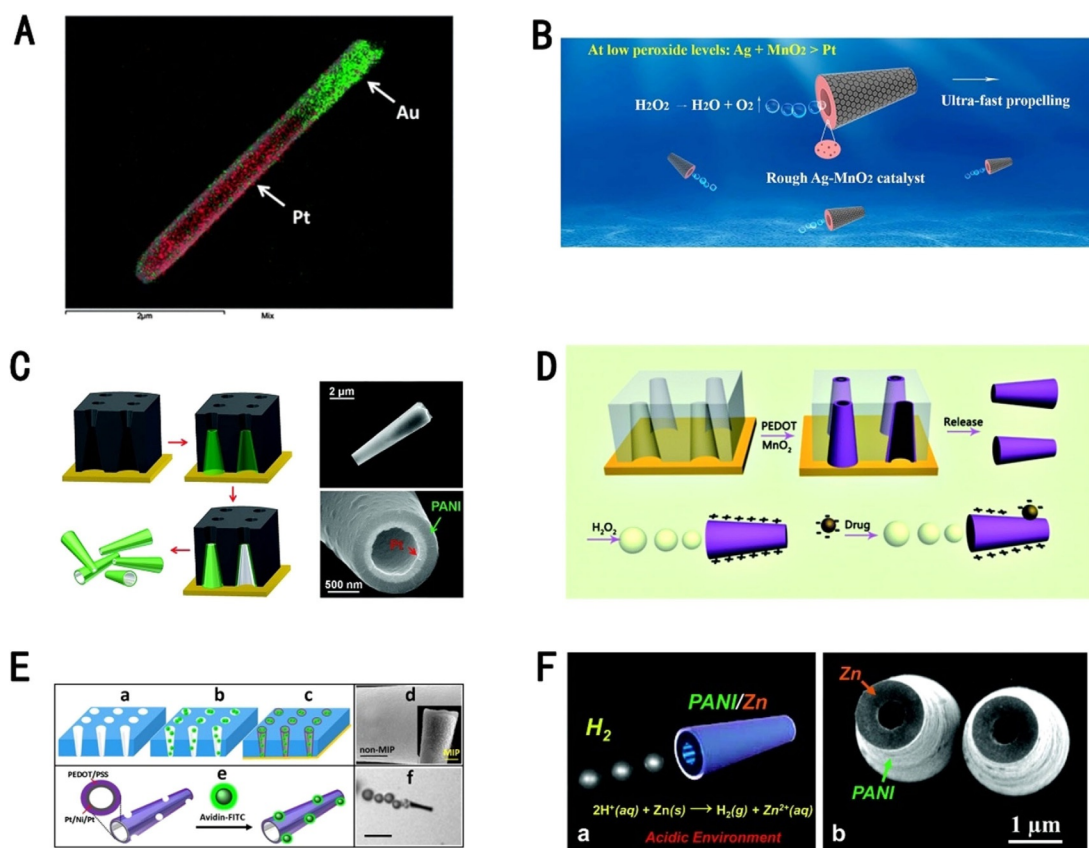


Figure 7. Membrane template-assisted electrodeposition of tubular Janus motors. A) Elemental mapping of an Au/Pt nanojet by means of SEM/energy-dispersive X-ray spectroscopy (EDX). Reproduced with permission from ref. [37]. Copyright 2013 Royal Society of Chemistry. B) Schematic illustration of Ag–MnO₂-based micromotors. Reproduced with permission from ref. [74]. Copyright 2013 Elsevier Ltd. C) Polycarbonate membrane-assisted fabrication and SEM images of conical polyaniline (PANI)/Pt microtubes. Reproduced with permission from ref. [75]. Copyright 2013 American Chemical Society. D) Schematic illustration of the preparation and modification process of poly(3,4-ethylenedioxythiophene) (PEDOT)/MnO₂ micromotors for drug delivery. Reproduced with permission from ref. [76]. Copyright 2016 Royal Society of Chemistry. E) Fabrication and characterization of a molecularly imprinted polymer (MIP)-based micromotor for protein transport. Reproduced with permission from ref. [77]. Copyright 2013 American Chemical Society. F) Schematic illustration of an acid-driven PANI–Zn microrocket, with a corresponding SEM image. Reproduced with permission from ref. [78]. Copyright 2012 American Chemical Society.

al chemical fuel. Zinc, as a biocompatible nutrient trace element, can be propelled in strongly acidic environments, such as the human stomach. The speed of this microtube increased with increasing acid concentration, and thus, showed pH-triggered motion.

2.2.2. Bipolar electrochemical deposition

Rather than employing a static membrane as a template, bipolar electrochemical deposition can be used for the design of Janus particles by inducing polarized deposition of conductive materials. It was reported for the first time by Fleischmann et al. for the synthesis of micrometer-sized particles in 1985.^[79] Briefly, a driving electric field was applied to a reactive solution containing conducting particles, which became a bipolar electrode or an array of bipolar electrodes.^[80] Oxidation and reduction reactions at opposite poles of the particles occurred if the induced polarization was high enough. The two driving electrodes are indispensable because they are connected to the external power supply and induce the interfacial reaction of bipolar electrodes. Because of unique structural characteristics, this material occupies an unparalleled position in the field of

materials science. Janus particles produced from bipolar electrochemical deposition are versatile with respect to a wide range of materials, sizes, and shapes of the particles. Therefore, the mass production of Janus particles can be achieved. A new technique of using two separated membranes between the anode and cathode to produce a reaction compartment containing substrates and reactants was also proposed.^[81] Indirect contact between the electrodes and objects enabled intense electric fields to be applied for a longer time and limited bubble formation. This appealing approach helps to realize the bulk synthesis of motors based on Janus objects.

2.2.2.1. Tubular Janus motors

If a conductive substrate was placed between two electrodes, asymmetric modification was realized through metal deposition at the cathodic side of the substrate. A magnetic Ni cap was asymmetrically deposited on one side of the carbon tube by means of capillary-assisted bipolar electrodeposition (Figure 8A).^[39] The carbon tubes and Ni salt were first introduced into the capillary without buffer solution to reduce the aggregation of carbon tubes. With the assistance of capillary forces,

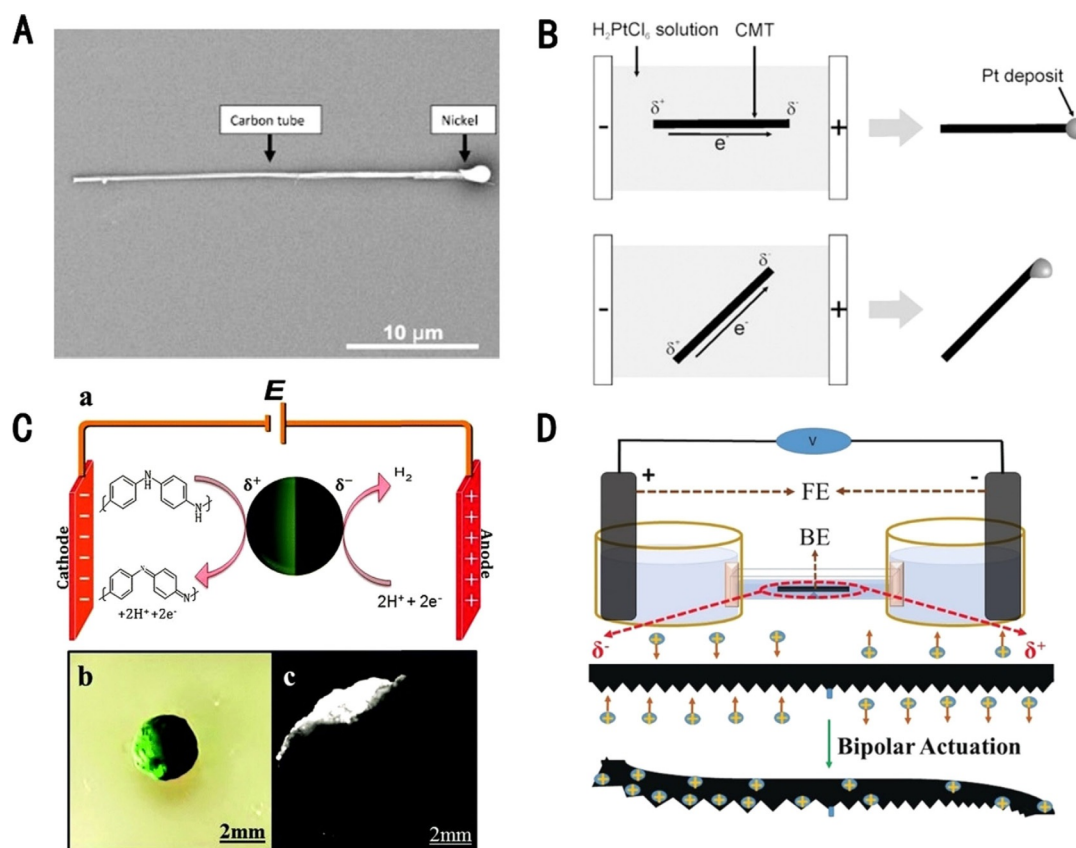


Figure 8. Bipolar electrochemical deposition of Janus motors. A) A SEM image of nickel modifying one end of a carbon nanotube. Reproduced with permission from ref. [39]. Copyright 2010 Elsevier Ltd. B) Schematic illustration of Pt deposition on one end of a carbon microtube. CMT = carbon microtube. Reproduced with permission from ref. [38]. Copyright 2010 Elsevier Ltd. C) Schematic illustration of an asymmetric hydrogel particle in an electric field. Reproduced with permission from ref. [40]. Copyright 2015 Royal Society of Chemistry. D) Schematic illustration of a polymer actuated in a bipolar electrochemical cell. FE = feeder electrode, BE = bipolar electrode. Reproduced with permission from ref. [83]. Copyright 2017 Wiley-VCH.

high voltages could be applied to induce polarization and the orientation of the tube. More importantly, no bubbles formed in the reaction chamber; thus ensuring the alignment of tubes in the electric field. Finally, Ni deposition at one side of the tube enabled manipulation under a magnetic field. A similar structure with Pt deposition at one end was reported later.^[38] Briefly, a sufficiently high electric field was applied to induce polarization of the carbon microtubes and a solution of H_2PtCl_6 was reduced at the anode to deposit Pt on one end of microtubes (Figure 8B). During deposition, an increase in the viscosity of solution helped to avoid possible rotation of the substrates in the high electric field. On the other hand, for the redox reactions to proceed smoothly, the conductivity of the substrate had to be higher than that in the surrounding medium. The prepared microtubes were able to propel linearly and circularly as a result of the decomposition of H_2O_2 by Pt. Additionally, bipolar electrochemistry was also used to induce the polarization of conducting objects, resulting in self-propulsion.^[82]

2.2.2.2. Other shapes

A Janus motor based on a soft hydrogel was developed through bipolar electrochemical deposition (Figure 8C).^[40] PANI

and alginate hydrogel were cross-linked into conductive beads in the presence of a low concentration of cross-linking agent. The formed soft beads were placed in an electrolyte solution and the asymmetric structure was realized by polarization under an external electric field. Upon loading with ethanol, the Janus hydrogel showed autonomous movement at the air/water interface through controlled release of the loaded solvent. In addition, wireless, electrochemically driven Ppy films were prepared recently (Figure 8D).^[83] The asymmetry was incorporated with Ppy films of different densities and porosities as a bilayer structure. The formed bilayer enabled the asymmetric oxidation/reduction of the polymer through bipolar electrochemistry, leading to the differential shrinking and swelling of both sides. Different scales of ring-like Janus objects could also be produced in bulk.^[84]

2.3. Assembly

Assembly is a spontaneous reorganization process induced by noncovalent interactions. This technique was first introduced to the fabrication of motors by the groups of Wilson^[41a] and He^[43] in 2012. Through assembly, soft materials, such as polymers and surfactants, can be used for the fabrication of micro- and nanomotors, both of which are sensitive to an external

stimulus; thus endowing the motors with versatility. The shape and size can be easily regulated for various purposes. These structures are easy for further modification and functionalization, which is important for effective encapsulation or incorporation of drugs or catalytic entities, such as enzymes and Pt. Moreover, employment of the assembly technique enables scaleup for the mass production of micro- and nanomotors.

2.3.1. Shape transformation method

Amphiphilic block copolymers, which have hydrophilic and -phobic polymer chains connected by covalent bonds, are ideal materials for self-assembly. Self-assembly can be well tuned by different parameters, such as block ratio and solvents, which results in various shapes, such as vesicles and micelles. As an example, amphiphilic block copolymers PEG-PS

were able to self-assemble into polymersomes. Upon dialysis, the organic solvent rapidly diffused outward from the hydrophobic PS part and resulted in a shape transformation into a stomatocyte, as proposed for the first time by the group of van Hest in 2010.^[85] Wilson and co-workers reported an efficient way to entrap Pt NPs within the nanocavities of stomatocytes for nanomotor applications (Figure 9A).^[41a] The stomatocyte has a unique asymmetric structure including an essential nanocavity, which can encapsulate Pt NPs or enzymes,^[86] to achieve self-propulsion upon decomposition of the substrate. It was crucial to control the sizes of the openings of cavities, not only for the diffusion of fuel and the release of products, but also for the retention of Pt NPs or enzymes. With this stomatocyte system, the chemotactic behavior was demonstrated to have an autonomous and directional movement towards the overproduction of H₂O₂ in neutrophil cells.^[87] Loaded with

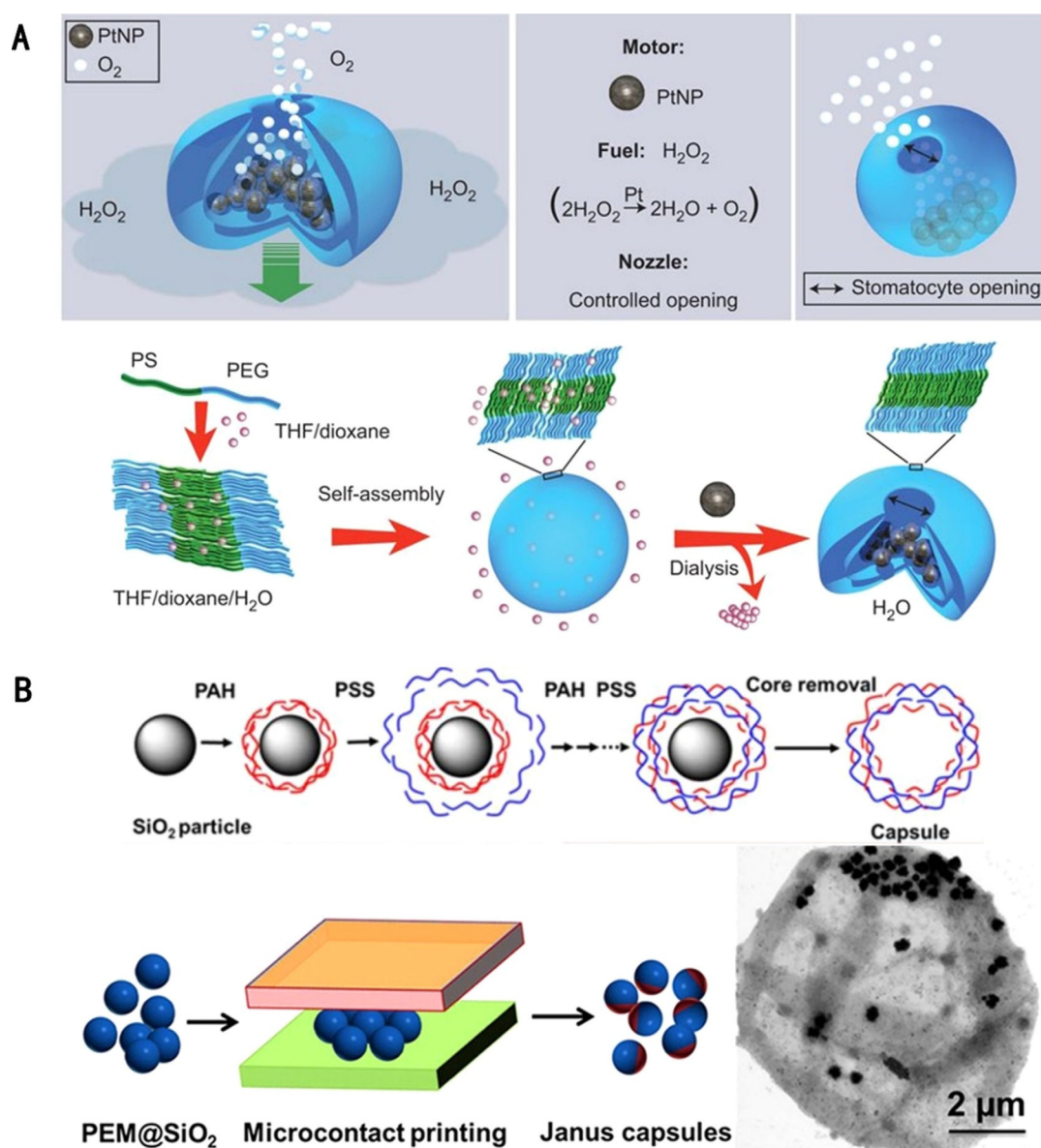


Figure 9. Assembly of Janus motors. A) Schematic illustration of Pt NPs entrapped in stomatocytes through the shape transformation method. Reproduced with permission from ref. [41a]. Copyright 2012 Nature Publishing Group. B) LbL assembly and microcontact printing of a Janus capsule. Reproduced with permission from ref. [43]. Copyright 2012 American Chemical Society.

doxorubicin (DOX), this nanomotor could act as an active drug-delivery system moving towards the targeted site. For more accurate control of the motion, the first chemically driven nanomotor with temperature-responsive speed regulation was reported recently.^[41b] Functionalized with a temperature-sensitive polymer brush on the surface of the nanomotors, the openings of the stomatocytes could be controlled by temperature. As the temperature was raised above the lower critical solution temperature (LCST) of the thermoresponsive block, the polymer brushes collapsed and produced a hydrophobic layer that covered the opening of cavities. A decrease of the size of the cavities prevented access of H₂O₂ fuel for the catalyst and regulated the speed of the movement of the nanomotors. A novel bioredox-responsive stomatocyte nanomotor system based on the disulfide bond between PEG and PS was reported.^[88] Degradation of the nanomotors and the release of loaded drugs could be triggered by the high concentration of endogenous glutathione in cells. Unfortunately, one of the components, PS, a glassy polymer, is non-biodegradable and non-biocompatible, and therefore, limits its further biomedical application. Poly(ϵ -caprolactone) (PCL) is a biodegradable polymer that is a good candidate for the construction of biodegradable motor systems. Stomatocyte structures composed of PEG-*b*-PCL and PEG-*b*-PS polymers were reported.^[89] This nanomotor system demonstrated properties of acid-induced degradation and the controlled release of the anticancer drug; thus showing great potential for drug-delivery applications. The entrapment of sensitive proteins or enzyme in the nanocavity of stomatocytes, while maintaining their efficiency and activity through shape transformation, was also described.^[86] In contrast to catalytic platinum motors, the resulting enzyme-driven nanomotors required lower fuel concentrations. More importantly, the encapsulation of enzymes in the cavities of stomatocytes was propitious to prevent their inactivation through the influence of the surroundings, which showed promise for application in biological media.

2.3.2. LbL assembly

LbL assembly was first reported by Decher in 1997.^[90] It is a versatile technique to deposit alternating layers of positively and negatively charged materials through electrostatic adsorption. To obtain the desired size and morphology of micro- and nanomotors, the number of layers needs to be modulated during the assembly process. Upon functionalization, motors can be endowed with the corresponding properties.

The first Janus micromotors fabricated through LbL assembly were developed in 2012 (Figure 9B).^[43] Five layers of oppositely charged PSS/PAH were adsorbed onto the surface of SiO₂ microparticles, followed by three centrifugation and washing steps. A polydimethylsiloxane (PDMS) stamp loaded with Pt NP ink was placed on top of the capsules to introduce the asymmetrical structure by microcontact printing. The resulting catalytic Janus capsules were obtained after removing the silica templates. Drugs can be encapsulated in micro- and nanomotors during LbL assembly to realize active drug delivery. Mag-

netic control can be further achieved by printing a magnetic component of iron oxide NPs onto micro- and nanomotors.

If the Pt layer was sputtered onto the LbL capsules to replace the printed Pt NPs, the asymmetrical Pt coating not only served as a catalyst for decomposition, but also as a photothermal agent for heat generation.^[44] The photothermal effect was able to lower the threshold of chemical fuel concentrations to propel Janus motors by remote NIR irradiation. Furthermore, gold nanorods can also be used for the photothermal activation of the motion of the assembled capsule, without additional chemical fuels.^[91] Gold-modified Janus motors based on LbL capsules can be further improved with a cloaked erythrocyte membrane, which would endow them with efficient motion in a physiological environment.^[92] The resulting Janus micromotor can be used for thermal-induced thrombus therapy. By using biocompatible and biodegradable components, these LbL Janus micromotors hold great promise in biomedical applications.

2.4. Biohybrids

Inspired by motile organisms in nature, scientists have combined different biological materials, such as enzymes, DNA, spermatozoa, and bacteria, to fabricate biohybrid micro- and nanomotors. Compared with inorganic catalysts, enzymes show higher catalytic efficiency and better biocompatibility, which makes them a more competitive component for use in motors. Combined with synthetic parts, this biohybrid approach provides a different strategy for the fabrication of Janus micro- and nanomotors.

Catalase is widely used as a substitute for inorganic catalysts in the design of self-propelled micro- and nanomotors. Janus capsules were fabricated through LbL assembly before the deposition of Cr, Ni, and Au layers successively. The Au layer was further functionalized with 3-mercaptopropionic acid for chemical immobilization of catalase (Figure 10A).^[93] These biohybrid motors could be magnetically navigated to a target site and the release of drugs triggered by NIR light. A similar Janus cluster motor driven by catalase through magnetic control was also demonstrated.^[45] In addition to catalase, other types of enzymes, such as urease and GOx, have been utilized recently. Three different kinds of self-driven, hollow, mesoporous, Janus nanomotors powered by biocatalytic reactions of catalase, urease, and GOx were reported (Figure 10B).^[94] Optical tweezers were introduced to determine the holding force required to counteract the force generated by a single Janus nanomotor.

Glucose is the major source of energy for normal physiological activities in cells. Decoration of GOx and catalase on the same side of the assembled Janus particles was demonstrated (Figure 10C).^[46] Self-propulsion was achieved by the gradual decomposition of glucose through the cascade reaction system of GOx and catalase. Although the driving force for these motors could not compete with individual catalase or inorganic catalysts, it was still an important step closer to practical use in the biomedical field. Urea is another energy source for self-driven micro- and nanomotors. A urea-powered and

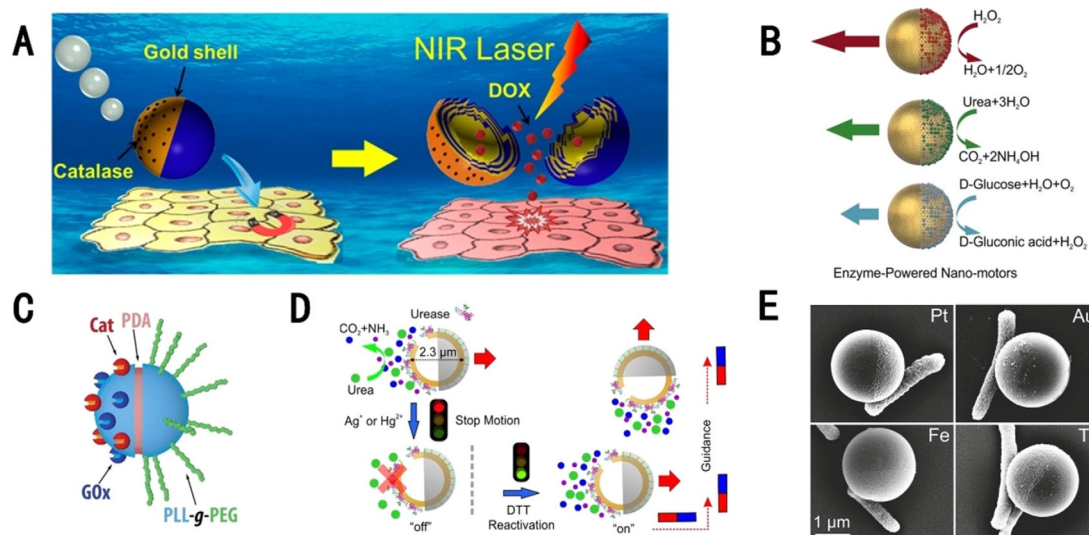


Figure 10. Biohybrid Janus motors. A) Schematic illustration of the use of a Janus capsule for drug delivery and light-triggered release. Reproduced with permission from ref. [93]. Copyright 2014 American Chemical Society. B) Schematic illustration of three different enzyme-powered Janus nanomotors. Reproduced with permission from ref. [94]. Copyright 2015 American Chemical Society. C) Schematic illustration of a Janus motor modified with GOx and catalase. PDA = poly(dopamine). Reproduced with permission from ref. [46]. Copyright 2015 American Chemical Society. D) Schematic illustration of motion control of a urea-powered Janus micromotor. DTT = dithiothreitol. Reproduced with permission from ref. [47]. Copyright 2015 American Chemical Society. E) SEM images of *Escherichia coli* attached to Janus particles. Reproduced with permission from ref. [48]. Copyright 2016 Wiley-VCH.

magnetically controlled Janus micromotor was demonstrated (Figure 10D).^[47] Through the addition of chemicals, the ON/OFF motion of micromotors could be precisely manipulated. Bacteria, as active swimmers, were also incorporated in the design of self-propelled motors (Figure 10E).^[48,95] Nonpathogenic *E. coli* showed a preference for attachment to the metal caps of Janus particles to power the motors in specific media. Sperm-driven micromotors for targeted drug delivery have been developed recently.^[96] Sperm are active swimmers and their hydrophilic heads have a high encapsulation capability for drugs. The hybrid motors were fabricated by trapping sperm inside the cavities of the tetrapods and could be targeted to tumor sites by guidance from an external magnetic field. These biohybrid motors offer a new strategy for application in living organisms.

3. Summary and Outlook

Micro- and nanomotors propelled by chemical fuel or external physical fields have attracted intense interest in the past decade. Despite different mechanisms of motion, these motors share one thing in common: an asymmetric field, such as gradients of concentration or temperature, for propulsion. In this sense, Janus motors with unique asymmetric structures are able to construct asymmetric fields in a straightforward way and induce the motion of motors. We presented four fabrication strategies for the design of Janus motors; all of which showed tremendous promise for practical applications. The motion of traditional self-propelled Janus motors relies heavily on a high concentration of toxic fuels, which hinders their biomedical applications. Therefore, fuel-free Janus motors powered by external stimuli seem to be an appealing substitution, but essential functional materials are required in the motor

systems. Moreover, specific equipment, such as that to generate high magnetic fields and strong electric fields, is complicated and cannot be manipulated widely. Therefore, we envision that different approaches should be integrated into one system to achieve spatial and temporal control of micro- and nanomotors in the future.

Although much progress in the fabrication of Janus motors has been achieved, challenges still exist. PVD is the most commonly used method to fabricate Janus motors. Micro- and nanomotors with similar geometry and morphology are easy to achieve, but PVD is expensive and requires strict conditions for fabrication. Electrochemical deposition is an ideal technology to fabricate Janus micro- and nanomotors based on metallic materials. By altering the electrochemical parameters, uniformity, such as thickness and morphology of the Janus motors, is easy to obtain; however, substrates must be conductive and adhesive. The resulting metal-based Janus nanomotor systems are inefficient for drug loading. Janus motors fabricated through assembly and as biohybrids are more convenient and lower in cost. Moreover, the assembly approach can be scaled up for bulk quantities. However, biodegradable systems with efficient motion in biological media still remain to be realized. For enzyme-powered biohybrid motors, considerable efforts are required to uncover the mechanism of motion and prevent the enzyme from inactivation.

The shape and size of Janus motors play important roles in their applications. Nonhollow, spherical, and cylindrical Janus motors have limited capacity for drug delivery. Although enzyme-powered Janus motors show higher catalytic efficiency and faster speed, their performance may be compromised if faced with the high viscosity of biological media. Therefore, cost-effective techniques for the fabrication of Janus motors with fast motion, as well as a high loading capacity, are still in

demand. Biocompatibility and biodegradability of Janus motors that can be controlled precisely are also indispensable for biomedical applications. Because the materials are of great significance in multifunctional Janus motors, new materials need to be explored for the novel design of Janus motors, especially in biomedical applications. We expect that Janus motors will act as intelligent micro- and nanorobots for drug delivery and noninvasive surgery in the near future.

Acknowledgements

This work was supported by the National Natural Science Foundation (31800835, 201805318) and the Natural Science Foundation of Guangdong Province (2018A030313521, 2018B030306007). Y.T. acknowledges financial support from the Pearl River Youth Scholar Funded Scheme. We thank Jing Liu for help with preparation of figures.

Conflict of interest

The authors declare no conflict of interest.

Keywords: Janus structures • motion control • nanostructures • self-assembly • synthesis design

- [1] R. D. Vale, R. A. Milligan, *Science* **2000**, *288*, 88–95.
- [2] R. F. Ismagilov, A. Schwartz, N. Bowden, G. M. Whitesides, *Angew. Chem. Int. Ed.* **2002**, *41*, 652–654; *Angew. Chem.* **2002**, *114*, 674–676.
- [3] W. F. Paxton, K. C. Kistler, C. C. Olmeda, A. Sen, S. K. St Angelo, Y. Cao, T. E. Mallouk, P. E. Lammert, V. H. Crespi, *J. Am. Chem. Soc.* **2004**, *126*, 13424–13431.
- [4] D. Pantarotto, W. R. Browne, B. L. Feringa, *Chem. Commun.* **2008**, 1533–1535.
- [5] W. Gao, A. Pei, J. Wang, *ACS Nano* **2012**, *6*, 8432–8438.
- [6] J. X. Li, P. Angsantikul, W. J. Liu, B. E. F. de Avila, S. Thamphiwatana, M. L. Xu, E. Sandraz, X. L. Wang, J. Delezuk, W. W. Gao, L. F. Zhang, J. Wang, *Angew. Chem. Int. Ed.* **2017**, *56*, 2156–2161; *Angew. Chem.* **2017**, *129*, 2188–2193.
- [7] a) Y. Tu, F. Peng, D. A. Wilson, *Adv. Mater.* **2017**, *29*, 1701970; b) T. Xu, W. Gao, L. P. Xu, X. Zhang, S. Wang, *Adv. Mater.* **2017**, *29*, 1603250.
- [8] P. G. de Gennes, *Angew. Chem. Int. Ed. Engl.* **1992**, *31*, 842–845; *Angew. Chem.* **1992**, *104*, 856–859.
- [9] A. Nourhani, D. Brown, N. Pletzer, J. G. Gibbs, *Adv. Mater.* **2017**, *29*, 1703910.
- [10] Y. R. Gao, F. Z. Mou, Y. Z. Feng, S. P. Che, W. Li, L. L. Xu, J. G. Guan, *ACS Appl. Mater. Interfaces* **2017**, *9*, 22704–22712.
- [11] W. Gao, A. Pei, R. Dong, J. Wang, *J. Am. Chem. Soc.* **2014**, *136*, 2276–2279.
- [12] C. R. Chen, E. Karshalev, J. X. Li, F. Soto, R. Castillo, I. Campos, F. Z. Mou, J. G. Guan, J. Wang, *ACS Nano* **2016**, *10*, 10389–10396.
- [13] a) D. A. Uygun, B. Jurado-Sanchez, M. Uygun, J. Wang, *Environ. Sci. Nano* **2016**, *3*, 559–566; b) D. Rojas, B. Jurado-Sánchez, A. Escarpa, *Anal. Chem.* **2016**, *88*, 4153–4160.
- [14] Y. Ge, M. Liu, L. M. Liu, Y. Y. Sun, H. Zhang, B. Dong, *Nano-Micro Lett.* **2016**, *8*, 157–164.
- [15] D. Vilela, M. M. Stanton, J. Parmar, S. Sanchez, *ACS Appl. Mater. Interfaces* **2017**, *9*, 22093–22100.
- [16] M. Xuan, J. Shao, C. Gao, W. Wang, Q. He, *Angew. Chem. Int. Ed.* **2018**, *57*, 12463–12467; *Angew. Chem.* **2018**, *130*, 12643–12647.
- [17] R. F. Dong, Q. L. Zhang, W. Gao, A. Pei, B. Y. Ren, *ACS Nano* **2016**, *10*, 839–844.
- [18] D. K. Zhou, Y. G. C. Li, P. T. Xu, N. S. McCool, L. Q. Li, W. Wang, T. E. Mallouk, *Nanoscale* **2017**, *9*, 75–78.
- [19] R. F. Dong, Y. Hu, Y. F. Wu, W. Gao, B. Y. Ren, Q. L. Wang, Y. P. Cai, *J. Am. Chem. Soc.* **2017**, *139*, 1722–1725.
- [20] Q. L. Wang, C. Wang, R. F. Dong, Q. Q. Pang, Y. P. Cai, *Inorg. Chem. Commun.* **2018**, *91*, 1–4.
- [21] L. F. Valadares, Y. G. Tao, N. S. Zacharia, V. Kitaev, F. Galembeck, R. Kapral, G. A. Ozin, *Small* **2010**, *6*, 565–572.
- [22] H. R. Vutukuri, Z. Preisler, T. H. Besseling, A. van Blaaderen, M. Dijkstra, W. T. S. Huck, *Soft Matter* **2016**, *12*, 9657–9665.
- [23] M. Xuan, X. Lin, J. Shao, L. Dai, Q. He, *ChemPhysChem* **2015**, *16*, 147–151.
- [24] J. G. Gibbs, N. A. Fragnito, Y. Zhao, *Appl. Phys. Lett.* **2010**, *97*, 253107.
- [25] T. C. Lee, M. Alarcóncorrea, C. Miksch, K. Hahn, J. G. Gibbs, P. Fischer, *Nano Lett.* **2014**, *14*, 2407.
- [26] J. A. Tejeda-Rodríguez, A. Núñez, F. Soto, V. García-Gradilla, R. Cadena-Nava, J. Wang, R. Vazquez-Duhalt, *ChemNanoMat* **2019**, *5*, 194–200.
- [27] C. R. Chen, S. S. Tang, H. Teymourian, E. Karshalev, F. Y. Zhang, J. X. Li, F. Z. Mou, Y. Y. Liang, J. G. Guan, J. Wang, *Angew. Chem. Int. Ed.* **2018**, *57*, 8110–8114; *Angew. Chem.* **2018**, *130*, 8242–8246.
- [28] R. Cheng, W. Huang, L. Huang, B. Yang, L. Mao, K. Jin, Q. Zhuge, Y. Zhao, *ACS Nano* **2014**, *8*, 7746–7754.
- [29] Y. He, A. J. Wu, Y. Zhao, *Nano Lett.* **2007**, *7*, 1369–1375.
- [30] a) J. G. Gibbs, Y. Zhao, *Small* **2010**, *6*, 1656–1662; b) J. G. Gibbs, Y. P. Zhao, *Small* **2009**, *5*, 2304–2308.
- [31] A. Ghosh, P. Fischer, *Nano Lett.* **2009**, *9*, 2243–2245.
- [32] S. Fournier-Bidoz, A. C. Arsenault, I. Manners, G. A. Ozin, *Chem. Commun.* **2005**, 441–443.
- [33] J. H. Guo, J. J. Gallegos, A. R. Tom, D. L. Fan, *ACS Nano* **2018**, *12*, 1179–1187.
- [34] W. Gao, S. Sattayasamitsathit, K. M. Manesh, D. Weihs, J. Wang, *J. Am. Chem. Soc.* **2010**, *132*, 14403–14405.
- [35] D. K. Zhou, L. Q. Ren, Y. G. C. Li, P. T. Xu, Y. Gao, G. Y. Zhang, W. Wang, T. E. Mallouk, L. Q. Li, *Chem. Commun.* **2017**, *53*, 11465–11468.
- [36] S. Ahmed, D. T. Gentekos, C. A. Fink, T. E. Mallouk, *ACS Nano* **2014**, *8*, 11053–11060.
- [37] G. Zhao, A. Ambrosi, M. Pumera, *Nanoscale* **2013**, *5*, 1319–1324.
- [38] Z. Fattah, G. Loget, V. Lapeyre, P. Garrigue, C. Warakulwit, J. Limtrakul, L. Bouffier, A. Kuhn, *Electrochim. Acta* **2011**, *56*, 10562–10566.
- [39] G. Loget, G. Larcade, V. Lapeyre, P. Garrigue, C. Warakulwit, J. Limtrakul, M. H. Delville, V. Ravaine, A. Kuhn, *Electrochim. Acta* **2010**, *55*, 8116–8120.
- [40] A. Srinivasan, J. Roche, V. Ravaine, A. Kuhn, *Soft Matter* **2015**, *11*, 3958–3962.
- [41] a) D. A. Wilson, R. J. Nolte, J. C. van Hest, *Nat. Chem.* **2012**, *4*, 268–274; b) Y. Tu, F. Peng, X. Sui, Y. Men, P. B. White, J. C. M. V. Hest, D. A. Wilson, *Nat. Chem.* **2017**, *9*, 480–486.
- [42] H. Choi, G.-H. Lee, K. S. Kim, S. K. Hahn, *ACS Appl. Mater. Interfaces* **2018**, *10*, 2338–2346.
- [43] Y. Wu, Z. Wu, X. Lin, Q. He, J. Li, *ACS Nano* **2012**, *6*, 10910–10916.
- [44] Y. Wu, T. Si, X. Lin, Q. He, *Chem. Commun.* **2015**, *51*, 511–514.
- [45] X. Ma, S. Sanchez, *Chem. Commun.* **2015**, *51*, 5467–5470.
- [46] P. Schattling, B. Thingholm, B. Stadler, *Chem. Mater.* **2015**, *27*, 7412–7418.
- [47] X. Ma, X. Wang, K. Hahn, S. Sanchez, *ACS Nano* **2016**, *10*, 3597–3605.
- [48] M. M. Stanton, J. Simmchen, X. Ma, A. Miguel-Lopez, S. Sanchez, *Adv. Mater. Interfaces* **2016**, *3*, 1500505.
- [49] J. Simmchen, J. Katuri, W. E. Uspal, M. N. Popescu, M. Tasinkevych, S. Sanchez, *Nat. Commun.* **2016**, *7*, 10598.
- [50] H. L. Yu, A. Kopach, V. R. Misko, A. A. Vasylenko, D. Makarov, F. Marchesoni, F. Nori, L. Baraban, G. Cuniberti, *Small* **2016**, *12*, 5882–5890.
- [51] C. Maggi, J. Simmchen, F. Saglimbeni, J. Katuri, M. Dipalo, F. De Angelis, S. Sanchez, R. Di Leonardo, *Small* **2016**, *12*, 446–451.
- [52] J. Katuri, D. Caballero, R. Voituriez, J. Samitier, S. Sanchez, *ACS Nano* **2018**, *12*, 7282–7291.
- [53] S. Das, E. B. Steager, M. A. Hsieh, K. J. Stebe, V. Kumar, *J. Micro-Bio Robotics* **2018**, *14*, 25–34.
- [54] A. F. Demirörs, M. T. Akan, E. Poloni, A. R. Studart, *Soft Matter* **2018**, *14*, 4741–4749.
- [55] S. S. Hu, S. B. Shao, H. Chen, J. J. Sun, J. Zhai, H. Y. Zheng, M. M. Wan, Y. H. Liu, C. Mao, J. Zhao, *J. Phys. Chem. C* **2018**, *122*, 9680–9687.
- [56] a) Y. Dou, C. A. Cartier, W. J. Fei, S. Pandey, S. Razavi, I. Kretzschmar, K. J. M. Bishop, *Langmuir* **2016**, *32*, 13167–13173; b) O. Ilıc, I. Kaminer,

- B. Zhen, O. D. Miller, H. Buljan, M. Soljacic, *Sci. Adv.* **2017**, *3*, e1602738; c) S. Simoncelli, S. Johnson, F. Kriegel, J. Lipfert, J. Feldmann, *ACS Photonics* **2017**, *4*, 2843–2851.
- [57] a) D. P. Singh, U. Choudhury, P. Fischer, A. G. Mark, *Adv. Mater.* **2017**, *29*, 1701328; b) Y. F. Wu, R. F. Dong, Q. L. Zhang, B. Y. Ren, *Nano-Micro Lett.* **2017**, *9*, 30; c) B. Jang, A. Hong, H. E. Kang, C. Alcantara, S. Charreyron, F. Mushtaq, E. Pellicer, R. Buchel, J. Sort, S. S. Lee, B. J. Nelson, S. Pane, *ACS Nano* **2017**, *11*, 6146–6154.
- [58] Q. L. Zhang, R. F. Dong, Y. F. Wu, W. Gao, Z. H. He, B. Y. Ren, *ACS Appl. Mater. Interfaces* **2017**, *9*, 4674–4683.
- [59] T. Li, A. Zhang, G. Shao, M. Wei, B. Guo, G. Zhang, L. Li, W. Wang, *Adv. Funct. Mater.* **2018**, *28*, 1706066.
- [60] F. Peng, Y. J. Men, Y. F. Tu, Y. M. Chen, D. A. Wilson, *Adv. Funct. Mater.* **2018**, *28*, 1706117.
- [61] Z. Wu, J. Troll, H.-H. Jeong, Q. Wei, M. Stang, F. Ziemssen, Z. Wang, M. Dong, S. Schnichels, T. Qiu, P. Fischer, *Sci. Adv.* **2018**, *4*, eaat4388.
- [62] D. Schamel, A. G. Mark, J. G. Gibbs, C. Miksch, K. I. Morozov, A. M. Le-shansky, P. Fischer, *ACS Nano* **2014**, *8*, 8794–8801.
- [63] a) H. R. Khan, K. Petrikowski, *Mater. Sci. Eng. C* **2002**, *19*, 345–348; b) M. Nishizawa, V. P. Menon, C. R. Martin, *Science* **1995**, *268*, 700–702; c) S. Valizadeh, J. M. George, P. Leisner, L. Hultman, *Thin Solid Films* **2002**, *402*, 262–271; d) J. D. Klein, R. D. Herrick, D. Palmer, M. J. Sailor, C. J. Brumlik, C. R. Martin, *Chem. Mater.* **1993**, *5*, 902–904.
- [64] J. C. Hulteen, C. R. Martin, *J. Mater. Chem.* **1997**, *7*, 1075–1087.
- [65] S. R. Nicewarner-Pena, R. G. Freeman, B. D. Reiss, L. He, D. J. Pena, I. D. Walton, R. Cromer, C. D. Keating, M. J. Natan, *Science* **2001**, *294*, 137–141.
- [66] W. Wang, W. Duan, A. Sen, T. E. Mallouk, *Proc. Natl. Acad. Sci. USA* **2013**, *110*, 17744–17749.
- [67] B. Jang, E. Gutman, N. Stucki, B. F. Seitz, P. D. Wendelgarcía, T. Newton, J. Pokki, O. Ergeneman, S. Pané, Y. Or, *Nano Lett.* **2015**, *15*, 4829.
- [68] M. Liu, F. Y. Wu, H. G. Piao, X. F. Huang, J. W. Cong, Z. C. Luo, L. Q. Pan, Y. M. Liu, *Appl. Phys. Express* **2017**, *10*, 045202.
- [69] S. Ahmed, W. Wang, L. J. Bai, D. T. Gentekos, M. Hoyos, T. E. Mallouk, *ACS Nano* **2016**, *10*, 4763–4769.
- [70] L. Q. Ren, D. K. Zhou, Z. M. Mao, P. T. Xu, T. J. Huang, T. E. Mallouk, *ACS Nano* **2017**, *11*, 10591–10598.
- [71] J. Wang, W. Gao, *ACS Nano* **2012**, *6*, 5745–5751.
- [72] Y. Mei, G. Huang, A. A. Solovev, E. B. Urena, I. Moench, F. Ding, T. Reindl, R. K. Y. Fu, P. K. Chu, O. G. Schmidt, *Adv. Mater.* **2008**, *20*, 4085–4090.
- [73] G. Zhao, M. Pumera, *RSC Adv.* **2013**, *3*, 3963–3966.
- [74] H. Ye, J. Kang, G. F. Ma, H. Q. Sun, S. B. Wang, *J. Colloid Interface Sci.* **2018**, *528*, 271–280.
- [75] W. Gao, S. Sattayasamitsathit, J. Orozco, J. Wang, *J. Am. Chem. Soc.* **2011**, *133*, 11862–11864.
- [76] L. L. Wang, J. Chen, X. M. Feng, W. J. Zeng, R. Q. Liu, X. J. Lin, Y. W. Ma, L. H. Wang, *RSC Adv.* **2016**, *6*, 65624–65630.
- [77] J. Orozco, A. Cortés, G. Cheng, S. Sattayasamitsathit, G. Wei, X. Feng, Y. Shen, J. Wang, *J. Am. Chem. Soc.* **2013**, *135*, 5336–5339.
- [78] W. Gao, A. Uygun, J. Wang, *J. Am. Chem. Soc.* **2012**, *134*, 897–900.
- [79] M. Fleischmann, J. Ghoroghchian, S. Pons, *J. Phys. Chem.* **1985**, *89*, 5530–5536.
- [80] S. E. Fosdick, K. N. Knust, K. Scida, R. M. Crooks, *Angew. Chem. Int. Ed.* **2013**, *52*, 10438–10456; *Angew. Chem.* **2013**, *125*, 10632–10651.
- [81] G. Loget, J. Roche, A. Kuhn, *Adv. Mater.* **2012**, *24*, 5111–5116.
- [82] a) G. Loget, A. Kuhn, *Nat. Commun.* **2011**, *2*, 535; b) J. Z. Jiang, M. H. Guo, F. Z. Yao, J. Li, J. J. Sun, *RSC Adv.* **2017**, *7*, 6297–6302.
- [83] B. Gupta, B. Goudeau, A. Kuhn, *Angew. Chem. Int. Ed.* **2017**, *56*, 14183–14186; *Angew. Chem.* **2017**, *129*, 14371–14374.
- [84] J. Roche, G. Loget, D. Zigah, Z. Fattah, B. Goudeau, S. Arbault, L. Bouffier, A. Kuhn, *Chem. Sci.* **2014**, *5*, 1961–1966.
- [85] K. T. Kim, J. Zhu, S. A. Meeuwissen, J. J. L. M. Cornelissen, D. J. Pochan, R. J. M. Nolte, J. C. M. van Hest, *J. Am. Chem. Soc.* **2010**, *132*, 12522–12524.
- [86] L. K. Abdelmohsen, M. Nijemeisland, G. M. Pawar, G. J. Janssen, R. J. Nolte, J. C. van Hest, D. A. Wilson, *ACS Nano* **2016**, *10*, 2652–2660.
- [87] F. Peng, Y. Tu, J. C. M. van Hest, D. A. Wilson, *Angew. Chem. Int. Ed.* **2015**, *54*, 11662–11665; *Angew. Chem.* **2015**, *127*, 11828–11831.
- [88] Y. Tu, F. Peng, P. B. White, D. A. Wilson, *Angew. Chem. Int. Ed.* **2017**, *56*, 7620–7624; *Angew. Chem.* **2017**, *129*, 7728–7732.
- [89] Y. Tu, F. Peng, A. A. M. André, Y. Men, M. Srinivas, D. A. Wilson, *ACS Nano* **2017**, *11*, 1957–1963.
- [90] G. Decher, *Science* **1997**, *277*, 1232–1237.
- [91] M. J. Xuana, J. X. Shao, X. K. Lin, L. R. Dai, Q. He, *Colloids Surf. A* **2015**, *482*, 92–97.
- [92] J. Shao, M. Abdelghani, G. Shen, S. Cao, D. S. Williams, J. C. M. van Hest, *ACS Nano* **2018**, *12*, 4877–4885.
- [93] Y. Wu, X. Lin, Z. Wu, H. Moehwald, Q. He, *ACS Appl. Mater. Interfaces* **2014**, *6*, 10476–10481.
- [94] X. Ma, A. Jannasch, U.-R. Albrecht, K. Hahn, A. Miguel-Lopez, E. Schaeffer, S. Sanchez, *Nano Lett.* **2015**, *15*, 7043–7050.
- [95] Z. H. Huang, P. Y. Chen, G. L. Zhu, Y. Yang, Z. Y. Xu, L. T. Yan, *ACS Nano* **2018**, *12*, 6725–6733.
- [96] H. Xu, M. Medina-Sanchez, V. Magdanz, L. Schwarz, F. Hebenstreit, O. G. Schmidt, *ACS Nano* **2018**, *12*, 327–337.

Manuscript received: February 23, 2019

Accepted manuscript online: April 4, 2019

Version of record online: May 21, 2019